**People's Democratic Republic of Algeria**

**Ministry of Higher Education and Scientific Research**

**University of Martyr Hamma Lakhdar**

**FACULTY OF TECHNOLOGIE**

**DEPARTMENT OF MECHANICAL ENGINEERING**

**Final research for the Master's degree**

**Topic**

# Model predictive control for PV water pumping systems based on synchronous Reluctance Motors

**Presented by:**

- **Bek Yahia**
- **Reguig saif Eddine**
- **Berrehaladem**

**Supervised by:**

**Dr. Mahmoudi Abdelkader**

Dr. Hamza Mesâi Ahmed **(Chairperson)**

Dr. Mahmoudi Abdelkader **(Supervisor)**

Dr. Chaabani Mohamed Essassi **(Examiner)**

2026/2025

ACKNOWLEDGEMENTS

In the name of Allah, the Most Gracious, the Most Merciful. All praise is due to Him for giving us the health and resolve to accomplish this work.

We owe a profound debt of gratitude to our supervisor, **Dr. Abdelkader Mahmoudi**.

His mentorship, technical insights, and unwavering encouragement were instrumental in the success of this thesis.

We are also highly honored by the presence of the jury members and thank them sincerely for their time and effort in reviewing our research.

To our colleagues, friends, and everyone who lent a helping hand along the way: thank you.

In The End , we offer our deepest thanks to our parents. This milestone is as much yours as it is ours; thank you for your unconditional belief in us.

# DEDICATION

In the name of Allah, the Most Gracious, the Most Merciful. All praise is due to Him.

We dedicate this humble work as a token of our profound respect, appreciation, and gratitude:

To our beloved fathers and mothers, whose endless sacrifices and prayers have lighted our path. To our brothers, sisters, and family members who supported us from near and far. And to everyone who contributed to the success of this thesis and holds a special place in our hearts.

# ABSTRACT

This work details a direct-coupled, battery-free solar water pumping system using a Synchronous Reluctance Motor, controlled by a Finite Control Set Model Predictive Controller (FCS-MPC) to maintain peak power and efficient water delivery even during sudden changes in sunlight.

**Keywords:** Photovoltaic Water Pumping System (PVWPS) · ynchronous Reluctance Motor (SynRM)· Maximum Power Point Tracking (MPPT)

**الملخص**

يتفصّل هذا العمل في نظام ضخ مياه شمسي مباشر الربط، خالٍ من البطاريات، باستخدام محرك تزامني مُمانع(SynRM) ، يتم التحكم فيه بواسطة متحكم تنبؤي بنموذج مجموعة التحكم المحدودة (FCS-MPC) بهدف الحفاظ على ذروة القدرة وكفاءة توصيل المياه حتى أثناء التغيرات المفاجئة في شدة الإشعاع الشمسي.

**الكلمات المفتاحية:** نظام ضخ المياه بالطاقة الكهروضوئية • (PVWPS) محرك تزامني مُمانع • (SynRM) تتبع نقطة القدرة القصوى(MPPT)

# TABLE OF CONTENTS

## CHAPTER 2 MODELING OF SOLAR PUMP BASED ON SYNRM MACHINE

## CHAPTER 3 FCS-MPC CONTROL STRATEGY AND MPPT



# List of Figures

# List of Tables



# List of equations

# List of Abbreviations

| | |
|---|---|
| **AC** | Alternating Current |
| **AM** | Air Mass |
| **BHJ-OSC** | Bulk Heterojunction Organic Solar Cell |
| **CCM** | Continuous Conduction Mode |
| **CdTe** | Cadmium Telluride |
| **CIGS** | Copper Indium Gallium Selenide |
| **CSI** | Current Source Inverter |
| **DC** | Direct Current |
| **DC-AC** | Direct Current to Alternating Current |
| **DC-DC** | Direct Current to Direct Current |
| **DCM** | Discontinuous Conduction Mode |
| **FCS-MPC** | Finite Control Set Model Predictive Control |
| **FF** | Fill Factor |
| **IGBT** | Insulated Gate Bipolar Transistor |
| **IM** | Induction Motor |
| **I-V** | Current-Voltage |
| **MOSFET** | Metal Oxide Semiconductor Field Effect Transistor |
| **MPP** | Maximum Power Point |
| **MPPT** | Maximum Power Point Tracking |

| | |
|---|---|
| **MTPA** | Maximum Torque Per Ampere |
| **P&O** | Perturb and Observe |
| **PMSM** | Permanent Magnet Synchronous Motor |
| **PV** | Photovoltaic |
| **PVG** | Photovoltaic Generator |
| **P-V** | Power-Voltage |
| **PWM** | Pulse Width Modulation |
| **RMS** | Root Mean Square |
| **SPD** | Surge Protection Device |
| **SPVWPS** | Solar Photovoltaic Water Pumping System |
| **STC** | Standard Test Conditions |
| **SWPS** | Solar Water Pumping System |
| **SynRM** | Synchronous Reluctance Motor |
| **TSM** | Trina Solar Module |
| **VSI** | Voltage Source Inverter |

# List of Symbols

| | |
|---|---|
| $A$ | Ideality factor of PV diode |
| $B$ | Viscous friction coefficient [N.m.s/rad] |
| $C$ | Output capacitance of boost converter [F] |
| $E$ | Photon energy [J] |
| $FF$ | Fill factor |
| $f$ | Frequency [Hz] |
| $G$ | Solar irradiance [W/m²] |
| $H$ | Total dynamic head [m] |
| $I$ | Electrical current [A] |
| $Iabc$ | Three-phase stator currents [A] |
| $Ib$ | Output current [A] |
| $Id$ | Direct-axis current [A] |
| $Idark$ | Dark saturation current [A] |
| $Iin$ | Input current [A] |
| $IL$ | Inductor current [A] |
| $Imp$ | Current at maximum power point [A] |
| $Iout$ | Output current [A] |
| $Ipv$ | Photovoltaic array current [A] |
| $Iq$ | Quadrature-axis current [A] |
| $Iph$ | Photo-generated current [A] |
| $Isc$ | Short-circuit current [A] |
| $J$ | Total moment of inertia [kg.m²] |
| $K$ | Proportionality constant of pump torque |
| $Kb$ | Boltzmann constant [J/K] |

| | |
|---|---|
| **L** | Inductance [H] |
| $N$ | Rotational speed [rpm] |
| $Np$ | Number of cells connected in parallel |
| $Ns$ | Number of cells connected in series |
| $P$ | Hydraulic pressure [Pa] |
| $Pb$ | Output power [W] |
| $Pdc$ | Direct current power [W] |
| $Pin$ | Incident light power [W] |
| $Pm$ | Maximum converted electrical power [W] |
| $Pmech$ | Mechanical power [W] |
| $Pout$ | Output power [W] |
| $Ppv$ | Photovoltaic output power [W] |
| $Q$ | Water flow rate [$m^3/s$] |
| $q$ | Elementary electron charge [C] |
| $R$ | Electrical resistance [Ω] |
| $Rp$ | Parallel (shunt) resistance [Ω] |
| $Rs$ | Series resistance [Ω] |
| $T$ | Temperature [°C or K] |
| $Te$ | Electromagnetic torque [N.m] |
| $TL$ | Load torque [N.m] |
| $Ts$ | Switching period [s] |
| $V$ | Electrical voltage [V] |
| $Va$ | Phase-a voltage [V] |
| $Vas$ | Stator phase-a voltage [V] |
| $Vb$ | DC-link voltage [V] |
| $Vbs$ | Stator phase-b voltage [V] |
| $Vc$ | Phase-c voltage [V] |
| $Vcs$ | Stator phase-c voltage [V] |
| $Vin$ | Input voltage [V] |
| $VL$ | Inductor voltage [V] |
| $Vmp$ | Voltage at maximum power point [V] |
| $Voc$ | Open-circuit voltage [V] |
| $Vout$ | Output voltage [V] |
| $Vpv$ | Photovoltaic array voltage [V] |
| $\omega m$ | Mechanical angular speed [rad/s] |
| $\eta$ | Conversion efficiency [%] |
| $\varepsilon$ | Albedo coefficient |
| $\lambda$ | Wavelength [m] |
| $\varphi$ | Magnetic flux [Wb] |
| $\rho$ | Fluid density [$kg/m^3$] |
| $\theta$ | Electrical angle [rad] |

# General Introduction

The continuous growth in global energy demand, combined with the progressive depletion of fossil fuel reserves and the increasing environmental concerns associated with greenhouse gas emissions, has accelerated the transition toward renewable energy sources. Among the available renewable technologies, solar photovoltaic (PV) energy has emerged as one of the most promising and sustainable solutions due to its abundance, cleanliness, reliability, and adaptability to both grid-connected and standalone applications.

In remote and isolated regions where access to conventional electrical networks is limited or unavailable, photovoltaic energy systems provide an effective alternative for supplying essential services such as lighting, irrigation, drinking water distribution, and agricultural pumping. In particular, photovoltaic water pumping systems (PVWPS) have attracted considerable attention because they offer an environmentally friendly and economically viable solution for water supply in rural and desert areas.

These systems eliminate the dependence on diesel generators, thereby reducing operational costs, maintenance requirements, and environmental pollution.
The performance and efficiency of photovoltaic pumping systems strongly depend on the effectiveness of their energy conversion chain and control strategy.
Traditional PV-powered pumping systems commonly employ induction motors or permanent magnet synchronous motors.

However, the Synchronous Reluctance Motor (SynRM) has recently emerged as an attractive alternative due to its simple rotor structure, absence of permanent magnets, high reliability, reduced maintenance requirements, and competitive efficiency. Furthermore, the SynRM presents a robust and cost-effective solution for variable-speed water pumping applications.
To maximize the extraction of solar energy under changing atmospheric conditions, Maximum Power Point Tracking (MPPT) techniques are widely implemented in photovoltaic systems. These techniques continuously adjust the operating point of the PV array to ensure operation at the Maximum Power Point (MPP), thereby improving the overall efficiency of the system. In addition, advanced control methods are required to achieve high-performance motor operation, minimize torque ripple, improve current tracking, and guarantee stable system dynamics.

Among modern control approaches, Finite Control Set Model Predictive Control (FCS-MPC) has gained significant interest in power electronics and electrical drive applications. This control strategy offers several advantages, including fast dynamic response, direct handling of system constraints, reduced dependence on modulation stages, and improved tracking performance. By predicting the future behavior of the system for all possible switching states and selecting the optimal voltage vector according to a predefined cost function, FCS-MPC provides superior control quality compared to conventional techniques.

The present thesis focuses on the modeling, simulation, and control of a standalone photovoltaic water pumping system powered by a Synchronous Reluctance Motor and controlled using a Finite Control Set Model Predictive Control strategy. The proposed system integrates a photovoltaic generator, a DC-DC boost converter with MPPT functionality, a voltage source inverter, a SynRM drive, and a centrifugal water pump. The objective is to develop a robust and efficient control architecture capable of ensuring optimal power extraction from the PV array while maintaining high-performance motor operation under varying solar irradiance and environmental conditions.

# Chapter 1

# STATE OF THE ART PHOTOVOLTAICSYSTEMS

## 1.1 Introduction :

Incorporating solar power into industrial applications has become an absolute necessity due to its limitless and eco-friendly nature. The main hurdle, however, remains the development of effective techniques to seamlessly replace traditional energy generation with these sustainable systems.

Directly transforming sunlight into electricity, the photovoltaic (PV) mechanism stands out as a leading method for capturing solar power. Generating clean energy is no longer a mere choice but a strict requirement in today's world, driven by the severe threats of greenhouse gas accumulation and widespread environmental contamination [1].

PV systems occupy a central role in the renewable energy sector, functioning as an infinite and pristine source of power. This technology has the capacity to meet the world's rapidly growing energy needs while concurrently limiting greenhouse gas outputs and alleviating ecological damage.

Despite the fluctuating nature of its energy production, photovoltaics provide a highly attractive alternative or addition to conventional power grids, largely owing to a series of unique benefits [2]:

- The systems are notably dependable and demand very little upkeep.
- Power generation relies completely on abundant, cost-free solar radiation.
- Combustible fuels are entirely unnecessary for operation.
- The technology is environmentally safe, producing no noise or polluting emissions during use.
- The functional longevity of these installations spans roughly two and a half decades.

This section of the text outlines the core principles governing photovoltaic setups. It delivers a brief summary of widespread solar cell types along with the physical arrangement of PV arrays.

Following this, the chapter examines and thoroughly details multiple strategies for modeling PV systems. After choosing the optimal mathematical representation, the governing equations for this framework are extensively described. Finally, simulations are executed using the chosen model under two separate environmental scenarios: shifting solar irradiance with a steady temperature, and stable irradiance combined with fluctuating temperatures.

### 1.2 The Definition of Photovoltaics :

Electrical power derived from photovoltaic solar energy is achieved by directly transforming solar irradiance. To enable this energetic transformation, semiconductor elements are utilized; silicon, in particular, acts as the primary base constituent required to manufacture photovoltaic solar panels.

From an etymological perspective, the expression "photovoltaic" represents an amalgamation of two separate linguistic roots:

- **Photo:** Derived from the Greek term *phos*, meaning "light."
- **Volt:** Serving as the conventional measurement for electromotive force and electrical potential, so named to recognize the early physicist Alessandro Volta.

### 1.3 The Historical Progression of Photovoltaics

The chronological advancement of this field is characterized by a variety of notable data points [3]:

- **1839:** The French physicist Edmond Beckerel uncovers the photovoltaic effect.
- **1875:** A paper discussing the photovoltaic effect within semiconductors is released by Werner von Siemens.
- **1954:** Three American investigators, Chapin, Fuller, and Pearson, successfully assemble a cell Photovoltaic.
- **1958:** A battery with 9 c/o efficiency is introduced, establishing the era wherein the first cell powered satellite harnessing solar energy is sent into space.
- **1973:** The initial residence sustained by photovoltaics is built University of Delaware.
- **1983:** Undertaking extensive journeys of 4000km, the inaugural photovoltaic-powered car travels in Australia.

**1.4 The Photovoltaic Phenomenon and the Physics of PV Cells:**

The operational efficiency of a solar cell is profoundly dictated by its thermal conditions. Theoretically, the absolute maximum voltage achievable by a photovoltaic unit corresponds directly to its bandgap energy, a theoretical limit strictly approached only at temperatures near absolute zero [4].

When the operating temperature of the cell climbs, it induces a concurrent contraction of both the bandgap and the electrical potential. Due to this compressed bandgap, freeing electrons from the semiconductor matrix demands less photonic energy, which consequently produces a marginal boost in the generated current. However, the ascending temperatures simultaneously trigger a much steeper and disproportionate collapse in voltage, meaning the total electrical power output of the device inevitably diminishes.

Fundamentally, the electrical yield of a photovoltaic unit demonstrates a direct proportional relationship with solar irradiance and an inverse relationship with thermal conditions. Consequently, territories characterized by frigid ambient climates combined with intense solar radiation emerge as the most advantageous geographical settings for deploying solar panel arrays [3].

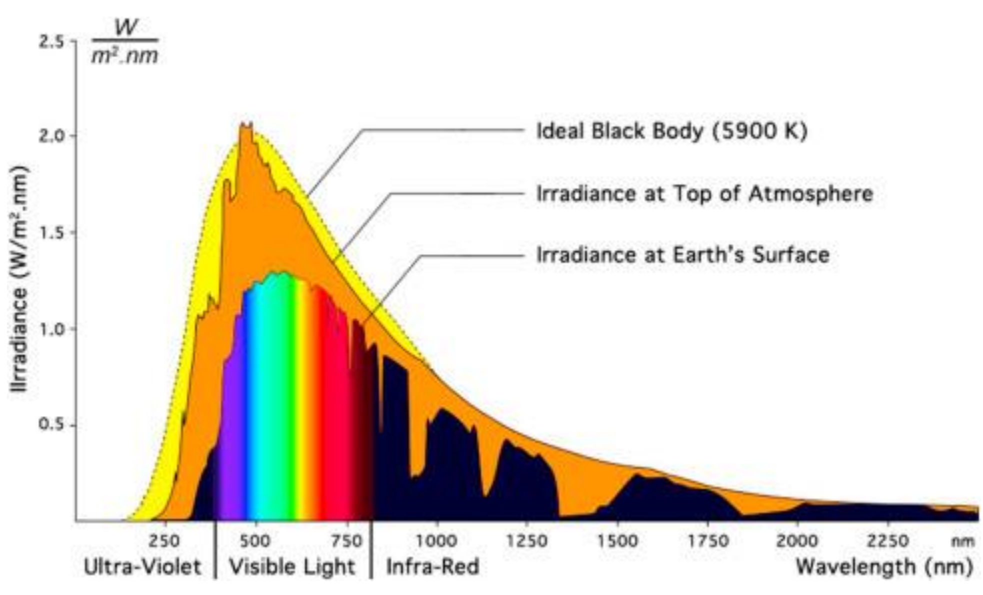


*Figure 1.1: Solar Radiation Spectrum*

### 1.5 Principles of Solar Energy :

The density of solar radiation striking the outermost layer of the atmosphere, oriented directly toward the sun, is defined as the solar constant. Typically, the magnitude of this illumination is established as being equal to $1360W/m^2$.

As this radiation propagates to ground level, atmospheric absorption causes the solar energy density to diminish to 1000 $W/m^2$. Furthermore, while conducting research on the effect Photoelectric, Albert Einstein concluded that light transcends a strictly wave-like nature; instead, the transmission of its energy occurs through individualized particles termed photons. The specific energy carried by a single photon is articulated by the subsequent relation [5]:

$$E = (h.c)/\lambda$$

$$h: Planck's\ constant\ [j.s\hat{}(-1)]. \quad (1.1)$$

$$C: the\ speed\ of\ light\ [m.s\hat{}\ (-1)].$$

$$\lambda: the\ wavelength\ [m].$$

Thus, the shorter the wavelength, the greater the energy of the photon

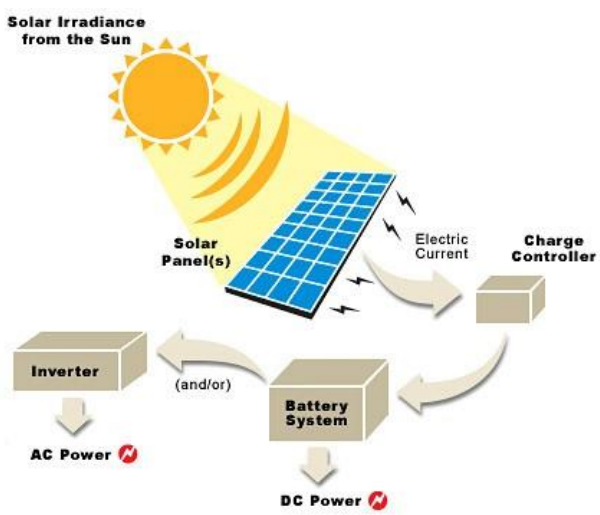


***Figure 1.2: Solar energy***

### 1.5.1Classifications of Solar Radiation :

- **Direct Radiation:** This component consists of solar flux composed of parallel rays that travel directly from the solar disc, passing through the Earth's atmosphere without experiencing any dispersion or scattering. [6]
- **Diffuse Radiation:** This fraction of solar energy reaches the terrestrial environment only after being subjected to atmospheric scattering and multiple reflective interactions. [6]
- **Reflected Radiation:** This represents the proportion of solar illumination that bounces off the Earth's surface. The intensity of this reflection is intrinsically linked to the physical composition of the terrain (e.g., sand, cloud cover, etc.). It is quantitatively defined by a specific surface-dependent metric known as the Albedo coefficient (ε), which is bounded by the parameters $0 \le \varepsilon \le 1$. [6]
- **Global Radiation:** A given receiving plane intercepts a total global irradiance, which is mathematically and physically defined as the aggregate superposition of the direct, diffuse, and reflected solar radiation components. [6]

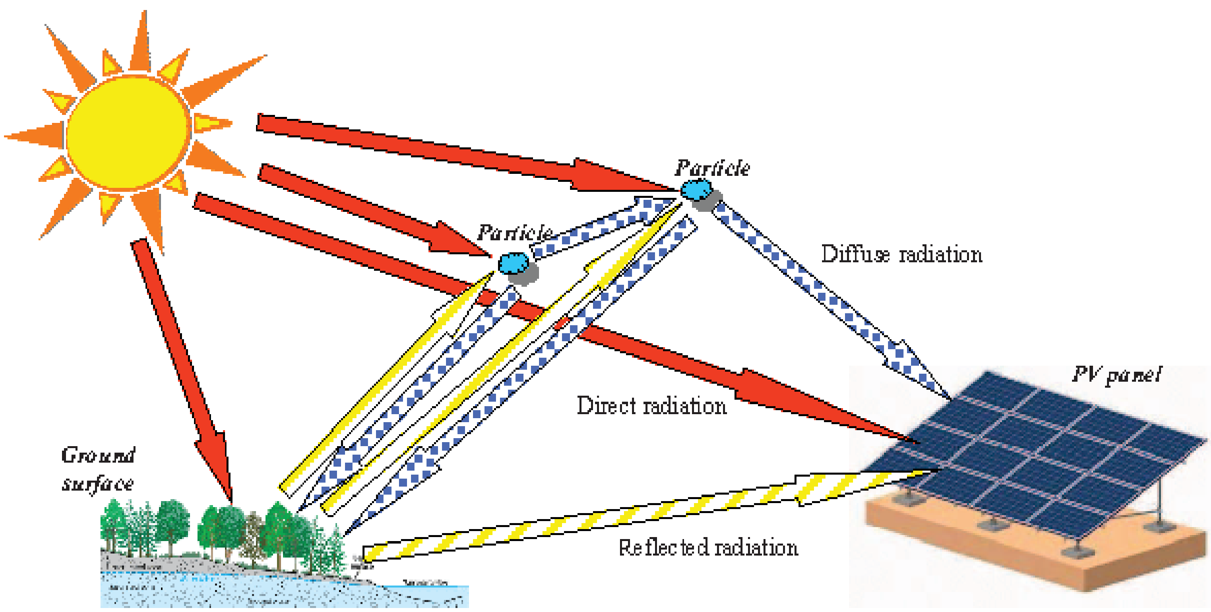


***Figure 1.3: Types of solar radiation (Direct, Diffuse and Reflected).***

### 1.6.Fundamental Operating Principles of a Photovoltaic Cell :

A photovoltaic (PV) cell, commonly designated as a solar cell, fundamentally consists of the integration of two distinct semiconductor materials, specifically structured as a P-doped layer and an N-doped layer. At the physical interface where these two strata converge, an inherent electric field is established, a phenomenon that persists continuously even when the device is situated in complete darkness.

When subjected to fluctuating intensities of solar illumination, discrete particles of light known as photons, provided they possess adequate energy, impact the atomic structure of the crystal lattice (Figure 1.4).

These incident photons provide the necessary excitation to propel electrons from the valence band of the semiconductor material into its conduction band, thereby engendering electron-hole pairs. Driven by the influence of the pre-existing potential barrier, these corresponding charge carriers systematically migrate and accumulate along the external boundaries of the P and N regions [2].

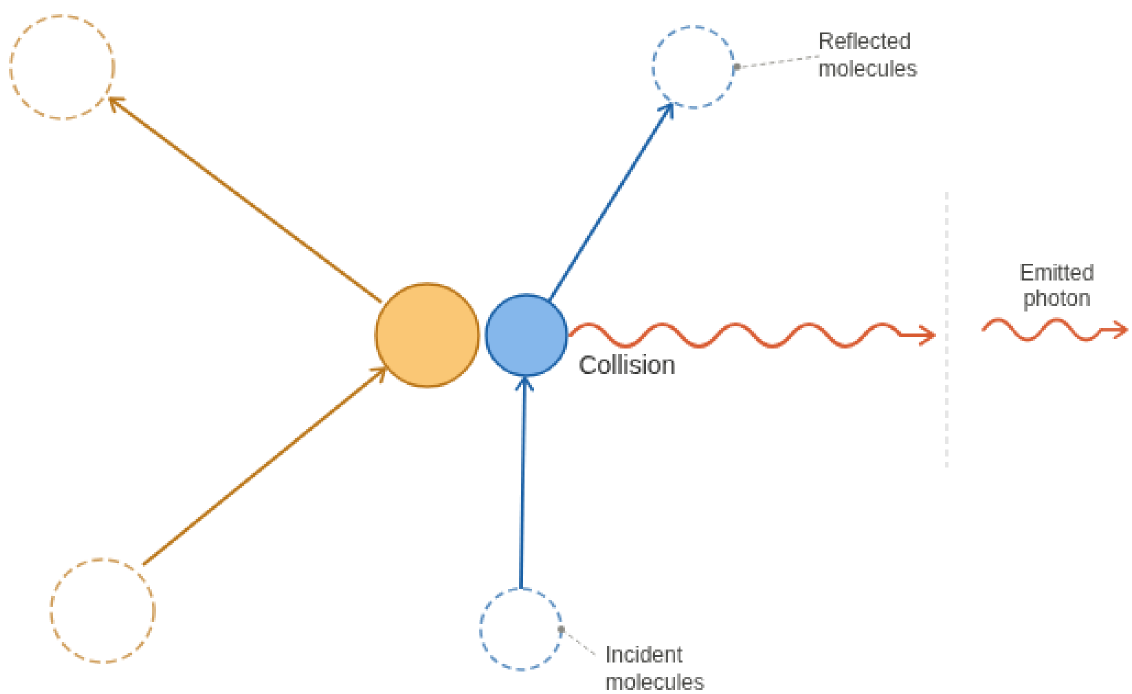


***Figure 1.4: Collision between a photon and an atom.***

Consequently, an electrical potential difference is established across the opposing surfaces of the device. Metallic contacts, positioned on both the anterior and posterior facets of the PV cell, are responsible for harvesting the separated electrons and holes, thereby delivering the resulting electrical current to an external load (Figure 1.5) [5].

Regardless of how highly energetic an incident photon may be, it is restricted to liberating only a single electron; any surplus energy is unavoidably dissipated as thermal waste. Structurally, the N-doped region is overlaid with a conductive metallic grid that functions as the cathode, whereas a continuous metal plate, serving as the back contact, coats the reverse side of the crystal to act as the anode. The overall thickness of this crystalline assembly is typically on the order of millimeters.

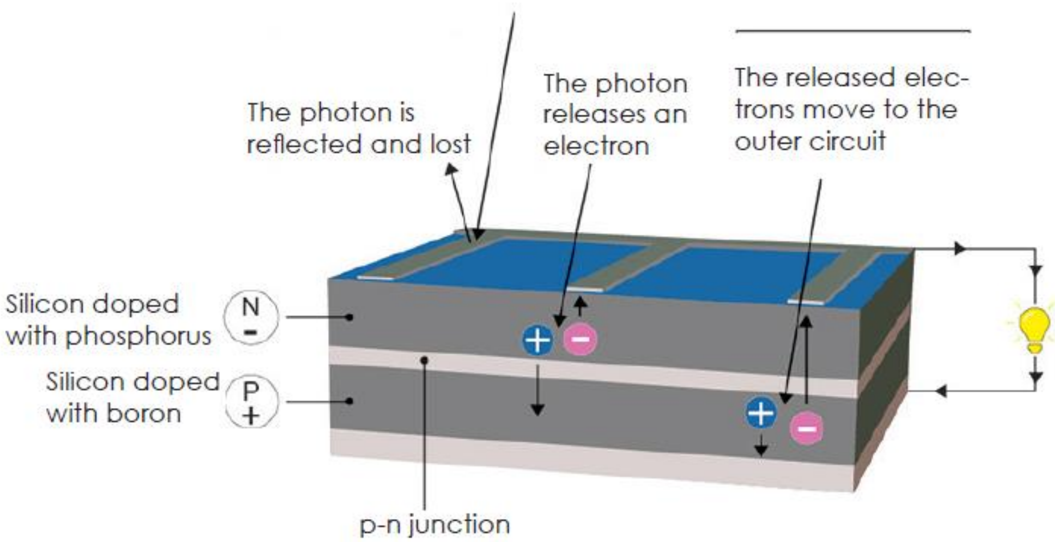


***Figure 1.5: Photovoltaic cell.***

### 1.6.1.Classifications of Extrinsic Semiconductors :

#### 1.6.1.1 P-Type Semiconductors :

The P-type variant constitutes a specific category of extrinsic semiconductors, engineered through the controlled introduction of a trivalent dopant into a purely intrinsic semiconductor matrix. Typical elemental candidates employed as these trivalent impurities include indium, gallium, and aluminum.

The deliberate insertion of such atoms into the crystalline lattice generates a structural deficit of electrons, thereby yielding a surplus of positively charged voids, which are designated as holes. Because of their inherent tendency to accept free electrons, these specific doping agents are characterized as acceptor impurities. As a direct consequence of this doping process, holes function as the predominant, or majority, charge carriers responsible for electrical conduction within a P-type semiconducting material [7].

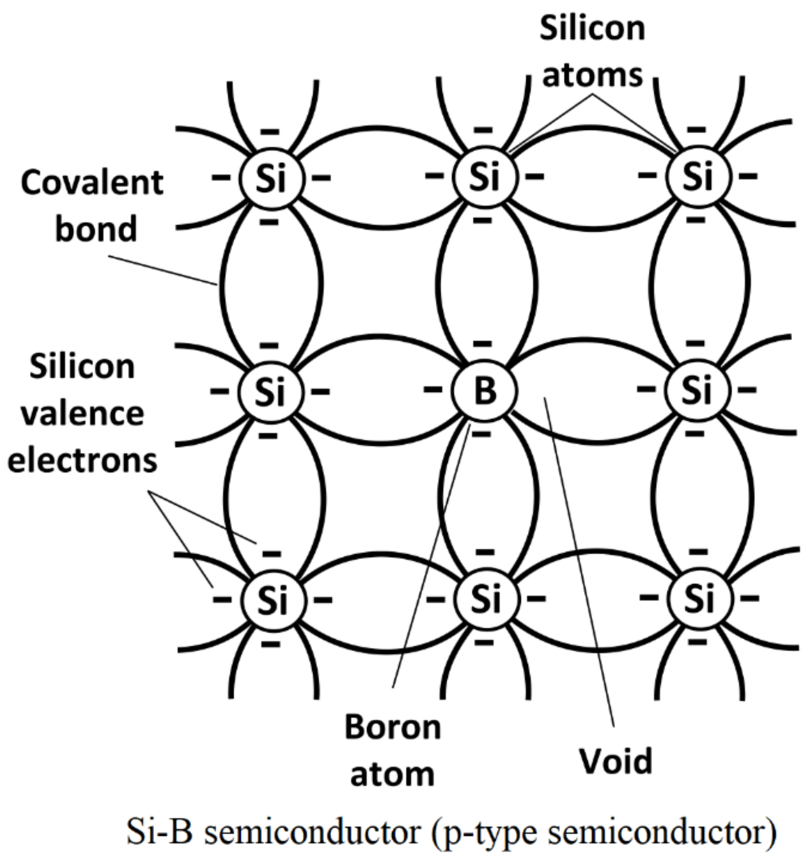


*Figure 1.6: Structure of p-type semiconductor*

**1.6.1.2.N-Type Semiconductors**

The N-type semiconductor represents another classification of extrinsic semiconductor materials, generated through the deliberate introduction of a pentavalent impurity into an intrinsic semiconductor base. Frequently utilized pentavalent doping agents include elements such as bismuth, arsenic, and antimony.

The incorporation of these specific atoms into the pristine semiconductor lattice introduces surplus electrons; consequently, these dopants are characterized as donor impurities. As a direct result of this physical mechanism, electrons serve as the predominant, or majority, charge carriers within the N-type semiconductor architecture [7].

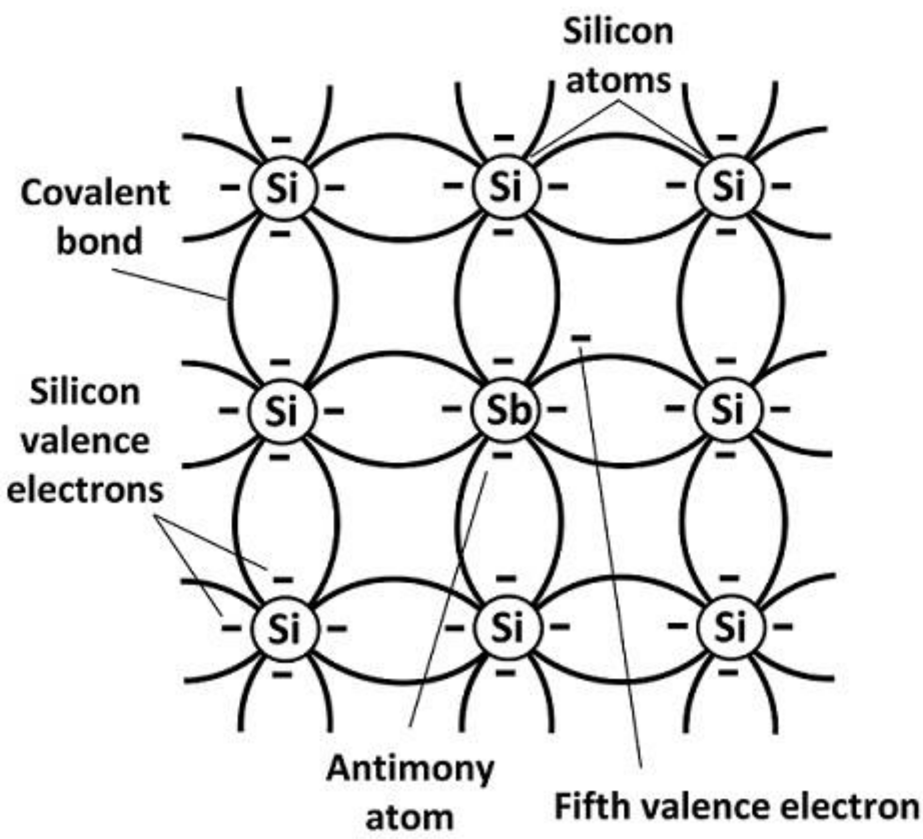


***Figure 1.7: Structure of n-type semiconductor***

**1.7.Structural Configuration of Photovoltaic Systems :**

The nominal capacity of photovoltaic systems is quantified by the peak direct current (DC) power generated by their underlying modules or cells when subjected to Standard Test Conditions (STC). These rigorous baseline parameters mandate an operating cell temperature of 25°C, an incident solar irradiance level of 1000 W/m2, and a spectral distribution corresponding to Air Mass 1.5. However, because practical field environments rarely replicate these idealized laboratory settings, the actual power yield of PV arrays typically functions at approximately 85% of their certified STC rating.

To scale the electrical output—specifically to attain amplified voltages, currents, and total power capacities—individual solar cells are electrically interconnected utilizing series and/or parallel circuit topologies. These assembled cellular networks are subsequently sealed within a durable, environmentally protective laminate to construct photovoltaic modules, which act as the primary building blocks of the entire PV infrastructure. Finally, when one or multiple modules are integrated into a cohesive, pre-wired framework designed for immediate field deployment, the resulting assembly is formally categorized as a photovoltaic panel. [5]

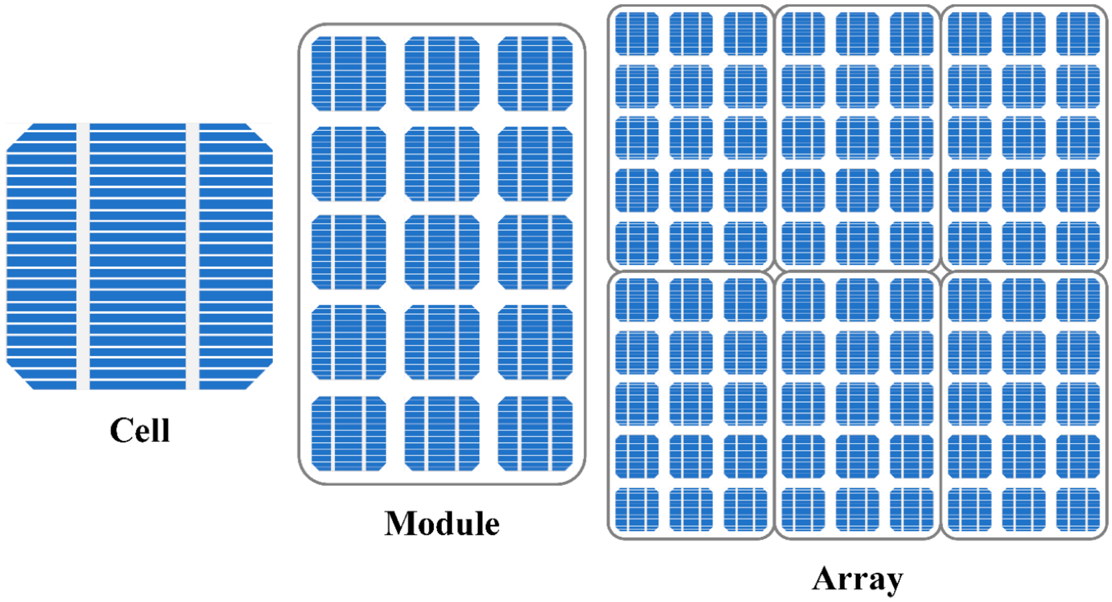


*Figure 1.8: photovoltaic cell, module and array*

## 1.8.The Generational Classifications of Photovoltaics :

The technological progression of photovoltaic (PV) cells is generally delineated into four primary categories: the first, second, third, and fourth generations. Every individual generational tier is distinguished by a unique set of intrinsic properties, technological benefits, and operational limitations.

### 1.8.1.FirstGenerationPhotovoltaics :

Currently representing the most widely deployed technology in the sector, crystalline silicon (c-Si) solar cells form the core of this initial category. The manufacturing protocol for these units necessitates the melting and subsequent crystallization of silicon to forge wafers of extraordinary purity.

From a performance standpoint, first-generation cells are highly regarded for their extended operational durability—typically surpassing a 25-year lifespan—and their commendable conversion efficiencies, which generally fall between 15% and 20%. Despite these technical merits, they remain the most financially demanding solar cells to fabricate, a direct consequence of the premium cost of raw silicon combined with an exceptionally energy-intensive production phase.

### 1.8.2.SecondGenerationPhotovoltaics :

Often referred to as thin-film solar cells, second-generation photovoltaic devices were engineered to serve as a more economically viable substitute for traditional crystalline silicon technologies. Their structural architecture involves the deposition of a microscopic layer of active photovoltaic material directly onto a supporting base substrate, which typically consists of glass or plastic. Prevalent examples within this specific category of thin-film technologies encompass cadmium telluride (CdTe), copper indium gallium selenide (CIGS), and amorphous silicon. Although these second-generation configurations generally yield lower energy conversion efficiencies—typically ranging between 10% and 15%—relative to first-generation models, this performance trade-off is offset by significantly reduced manufacturing expenditures.

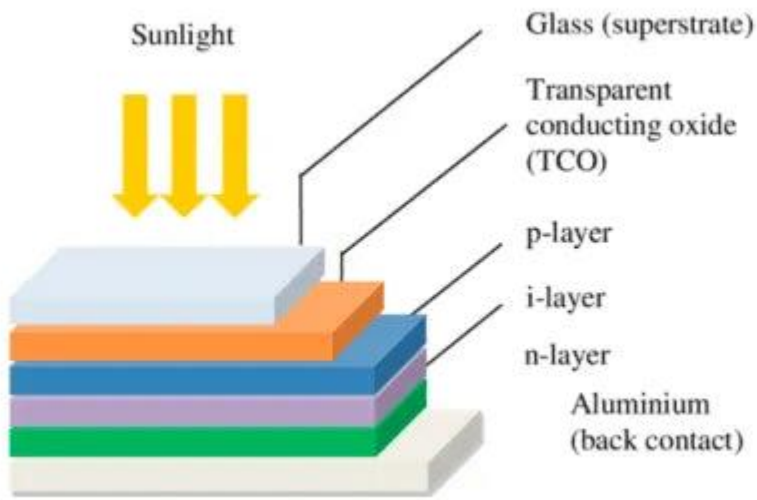


***Figure 1.9: Second Generation Solar Cell***

### 1.8.3. Third-Generation Photovoltaics :

Although currently in ongoing phases of research and development, third-generation solar cells possess the theoretical capacity to achieve superior conversion efficiencies and lower manufacturing expenditures compared to their first- and second-generation predecessors. This category encompasses an array of novel materials and innovative technological approaches, notably featuring organic solar cells, dye-sensitized solar cells, and perovskite-based architectures. While these advanced photovoltaic configurations remain primarily within nascent developmental stages, they harbor the transformative potential to fundamentally revolutionize the global solar energy landscape. [6]

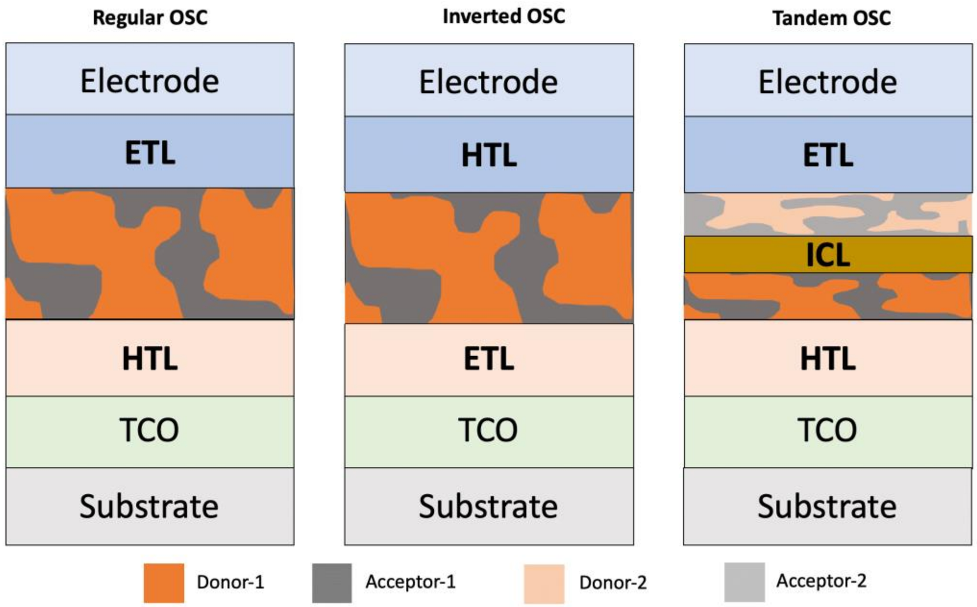


*Figure 1.10: Schematic diagram of typical BHJ-OSC (Regular OSC, inverted OSC and tandem OSC) [23]*

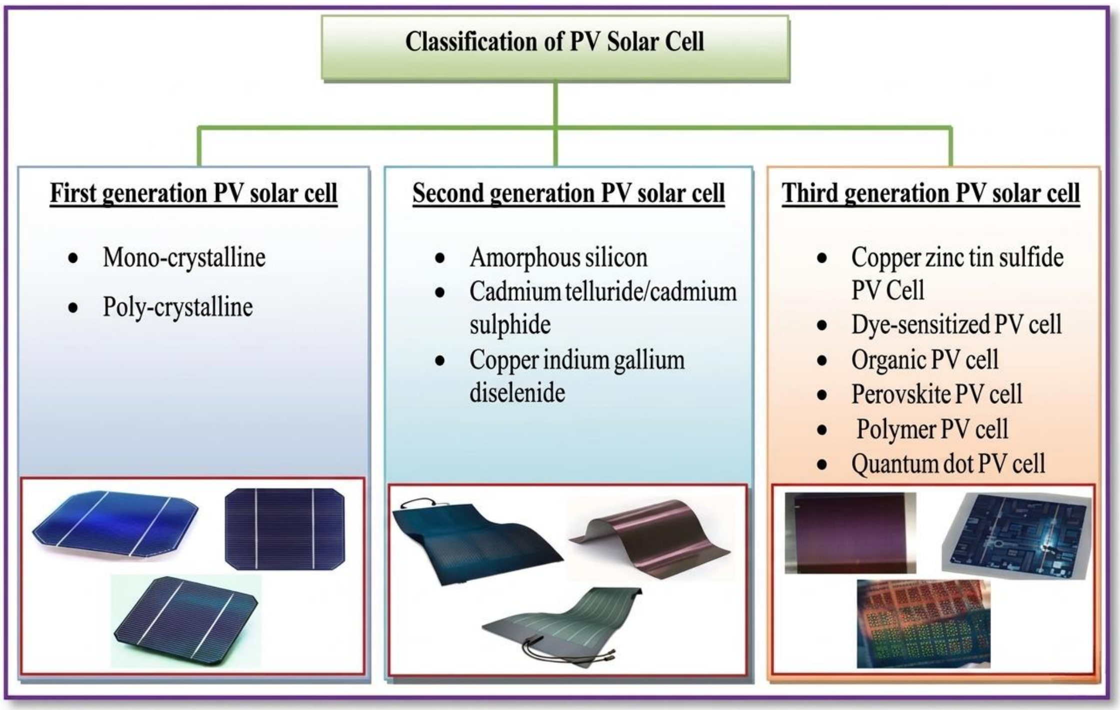


*Figure 1.11: The three generations of solar photovoltaic (PV) cells*

### 1.9. Synoptic Diagram of the Photovoltaic Conversion Chain :

The entire operational sequence of a photovoltaic (PV) system can be effectively represented through a synoptic diagram. This conceptual schematic provides a streamlined overview of the primary subsystems and their functional interdependencies. The fundamental constituents of this conversion chain are delineated as follows [8]:

- **PV Panel:** Serving as the foundational component, this module is composed of an array of interconnected solar cells. Its primary function is the direct transduction of incident solar radiation (photons) into direct current (DC) electrical energy utilizing the photovoltaic effect.
- **Maximum Power Point Tracking (MPPT) Unit (Optional):** This specialized electronic controller is engineered to maximize the power yield extracted from the photovoltaic array. It achieves this by dynamically modulating the operational voltage and current to continuously align with the maximum power point (MPP), thereby compensating for environmental fluctuations such as variations in thermal conditions and solar irradiance.
- **DC-DC Converter (Optional):** Within certain architectural configurations, a direct current to direct current converter is integrated to regulate and scale the voltage output from the PV array, ensuring compatibility with the specific input voltage parameters demanded by the downstream inverter or an interconnected DC load.
- **DC-AC Inverter:** This essential component is responsible for the inversion of the DC power supplied by the photovoltaic panels (or the intermediary DC-DC converter) into alternating current (AC). This synthesized AC power is subsequently suitable for conventional consumption by standard appliances or for direct synchronization and injection into the utility grid.
- **Load:** This element denotes the terminal apparatus or broader network that consumes the final synthesized AC electrical power. Typical examples encompass residential electrical appliances, illumination infrastructure, or the broader commercial electrical grid.

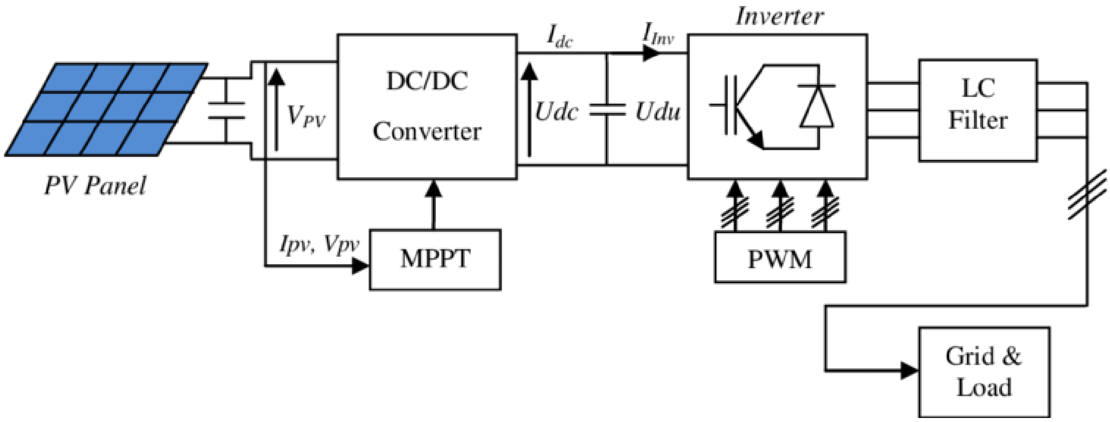


***Figure 1.12: Synoptic diagram of the photovoltaic conversion chain. [23]***

**1.10. The Photovoltaic Cell :**

Photovoltaic cells whose nomenclature is derived from "photon" (representing a discrete quantum of light energy) and "volt" (denoting the standard measurement of electrical potential)constitute fundamental electronic devices fabricated from semiconductor materials, most prevalently utilizing silicon across its various morphological states.

These components function by directly transmuting incident luminous energy into electrical power by means of the photovoltaic effect. Given that solar radiation serves as the primary and most abundant source of this requisite light energy, these devices are colloquially and widely designated as solar cells.

**1.11. The Photovoltaic Module :**

Because an isolated photovoltaic cell inherently generates a relatively modest electrical output, multiple cells must be systematically interconnected utilizing series and parallel circuit topologies. This strategic aggregation forms a cohesive PV module capable of delivering the requisite power capacity for practical applications.

From a commercial and standardization standpoint, a photovoltaic module is typically classified according to its peak direct current (DC) power yield when evaluated under Standard Test Conditions (STC). These rigorous baseline parameters are universally defined by an incident solar irradiance of 1000 W/m² coupled with an internal cell operating temperature of 25°C [5].

The corresponding electrical equivalent circuit of a PV module is visually represented in Figure 1.13. Assuming strict structural and operational uniformity among all constituent cells within the array, the inherently nonlinear current-voltage (I-V) characteristic of the complete module is mathematically modeled by the subsequent equation [5]:

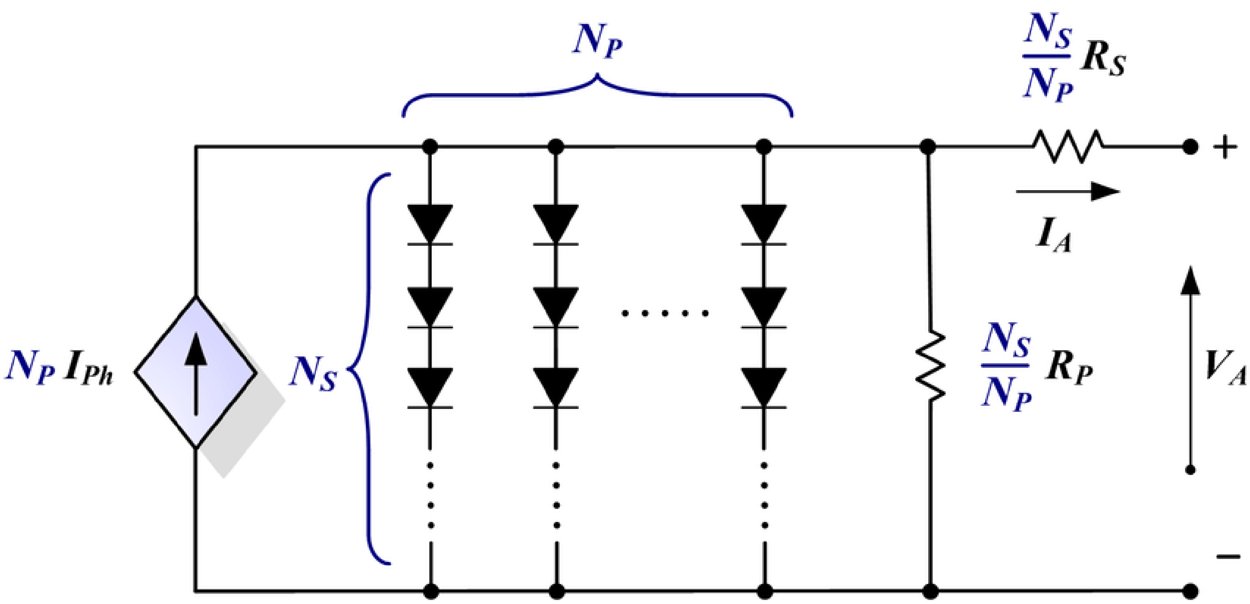


***Figure 1.13: The equivalent circuit of a PV module.***

**Where:**

$I_A$**:** is the module output current (A).

$V_A$: is the module output voltage (V).

$N_s$: is the number of cells connected in series

$N_P$: is the number of cells connected in parallel

The specific photovoltaic array selected for the scope of this research is the Trina Solar TSM-250PA05.08 model. The fundamental current-voltage (I-V) and power-voltage (P-V) performance trajectories for this particular module, evaluated under Standard Test Conditions (STC), are graphically depicted in Figure 1.14.

During active operation, a PV module is capable of generating electrical power at any specific coordinatedesignated as an operating pointsituated along its continuous I-V curve. However, the overall performance profile and efficiency limits of the module are intrinsically defined by three critical operational thresholds: the maximum power point, the short-circuit current, and the open-circuit voltage.

- **Maximum Power Point (MPP):** This designates the optimal coordinate along the I-V curve where the photovoltaic module yields its absolute highest electrical power output.
- **Short-Circuit Current (Isc):** This specific operating point is characterized by a state where the voltage across the module's output terminals is effectively zero, resulting in the maximum theoretical continuous current flow, defined as the short-circuit current (Isc).
- **Open-Circuit Voltage ($V_{OC}$) :** This specific operational state manifests when the electrical current flowing through the terminals of the PV panel is exactly zero, yielding the maximum available electrical potential, which is formally defined as the open-circuit voltage**($V_{OC}$)**

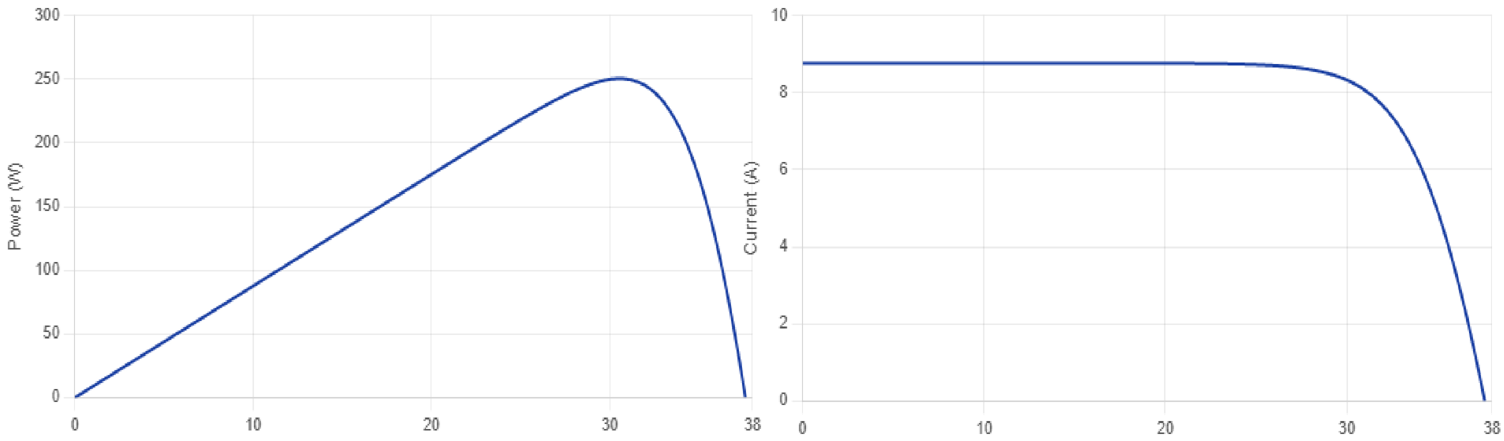


***Figure 1.14: (a) I-V and (b) P-V characteristics of the solar Trina Solar TSM-250PA05.08 PV model under STC***

### 1.12. Structural Composition of a Photovoltaic Module :

A photovoltaic cell is an advanced semiconductor instrument specifically engineered to transduce incident solar radiation directly into direct current (DC) electrical energy. Given that natural sunlight overwhelmingly constitutes the primary radiation source for this process, these devices are universally identified as solar cells.

From a hierarchical manufacturing and integration perspective, single, individual PV cells function as the fundamental elemental units. These isolated components are systematically aggregated and interconnected to construct larger, integrated structures known as PV modules. In turn, these modules act as the standardized structural foundationsor building blocksrequired for the assembly of expansive photovoltaic arrays and the deployment of comprehensive, large-scale PV systems (refer to Figure 1.15 for visual context) [10].

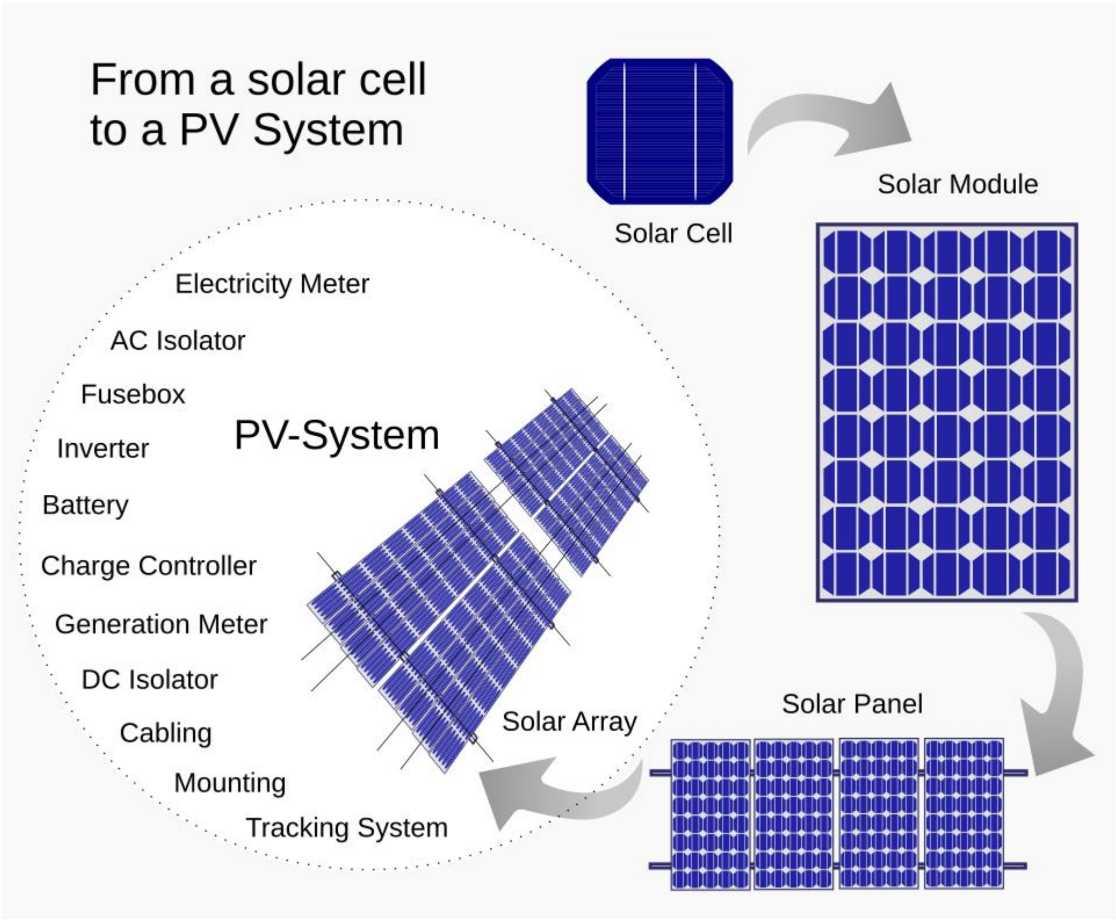


***Figure 1.15: The Composition of a Solar Cell.***

## 1.13. Interconnection of Photovoltaic Cells and Module Assembly :

Irrespective of its geometric configuration, typically circular or rectangular, the individual solar cell functions as the foundational building block of any photovoltaic architecture. The systematic aggregation of these discrete cells constitutes a solar module, wherein the operational units are electrically networked and hermetically encapsulated to ensure robust protection against environmental degradation. Subsequently, the integration of multiple distinct modules forms a comprehensive solar panel.

When organized into larger macro-structures, numerous panels coalesce to establish a complete solar system, commonly referred to as a photovoltaic array. Such expansive architectures

frequently incorporate auxiliary peripheral subsystems, including electrical protection mechanisms, charge regulators, energy storage reservoirs (batteries), and sophisticated diagnostic and telemetry instrumentation [3].

Given that the baseline power output of an isolated solar cell is intrinsically marginal, it is an engineering necessity to electrically couple numerous cells possessing congruent operational characteristics. These assembled arrays are then encased within durable polymeric laminates to synthesize a commercially viable PV module. The subsequent sections delineate the primary circuit topologies utilized for grouping and interconnecting these solar cells.

**1.13.1. Series Circuit Configuration :**

Within a series interconnection topology, an identical electrical current propagates sequentially through each linked cell, as illustrated in Figure 1.16. The cumulative performance characteristic of this specific configuration is mathematically and functionally derived by adding the individual voltage potentials of each constituent cell while maintaining a constant, uniform current.

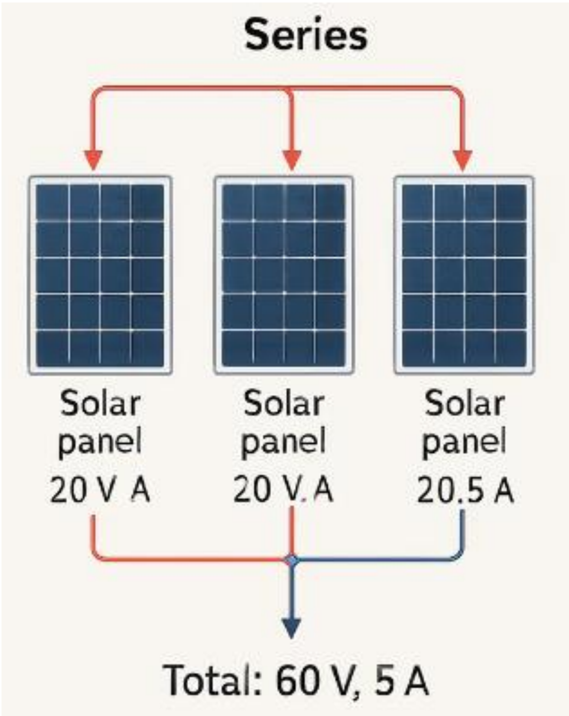


***Figure 1.16: Series Connection of cells***

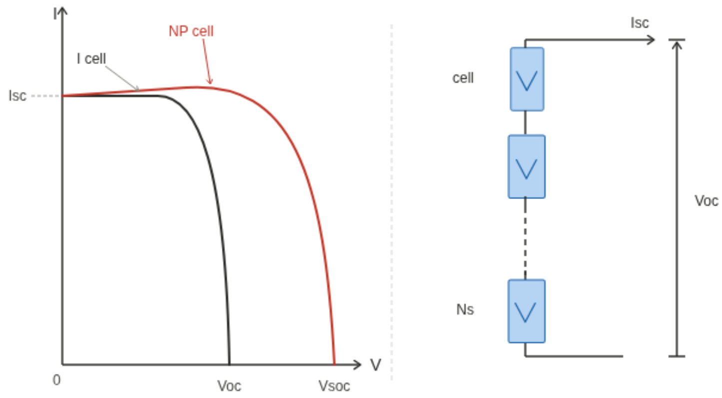


*Figure 1.17: Characteristics resulting from a grouping of Ns cell in series*

### 1.13.2. Parallel Circuit Configuration :

The operational characteristics inherent to a parallel interconnection of solar cells function as the precise electrical dual to those observed in a series configuration. Within a parallel topology, the electrical potential (voltage) remains uniformly constant across all interconnected units, while the total output current is the sum of the individual cell currents. This fundamental principle is visually demonstrated in Figure 1.18, which additionally illustrates a hybrid or mixed circuit architecture consisting of two distinct series-connected strings systematically wired in parallel.

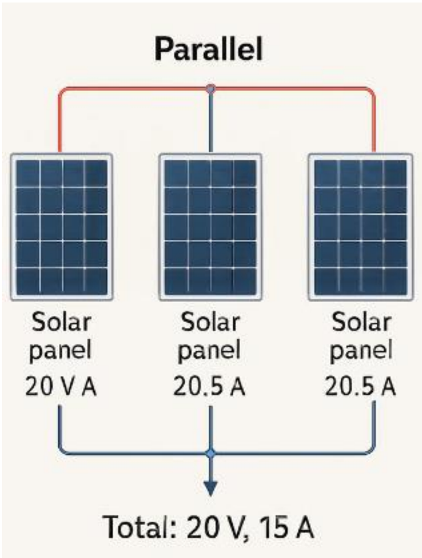


*Figure 1.18: Parallel Connection of cells.*

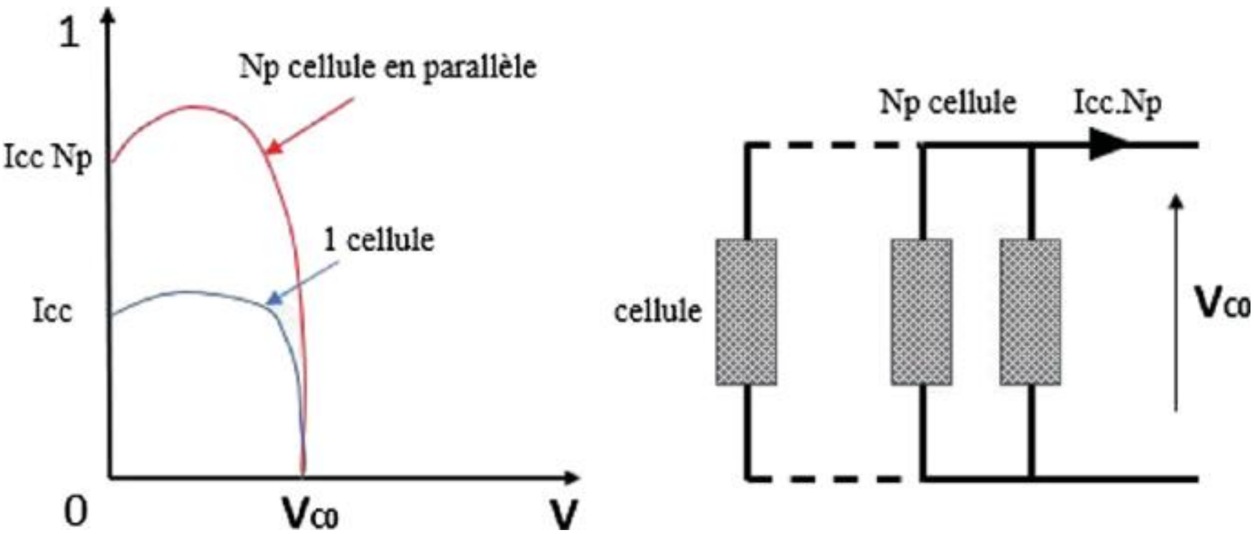


*Figure 1.19: Characteristics resulting from a grouping of Np cells in parallel*

### 1.14. Installation Protocols and Safeguards for Photovoltaic Modules :

#### 1.14.1. Strategic Site Selection

The physical deployment of photovoltaic arrays necessitates an environment strictly devoid of potential shading from adjacent obstacles (such as foliage or architectural structures) throughout the entire diurnal cycle, continuously accounting for the shifting solar trajectories across all seasons. Furthermore, to effectively mitigate thermal accumulation, the modules must be mounted with adequate spatial clearance from their supporting substructures. This design consideration facilitates natural convective cooling, thereby limiting heat retention and preserving optimal operational efficiency. [8]

#### 1.14.2. Optimization of Panel Inclination :

To achieve a balanced and optimized annual energy yield that accommodates both summer and winter extremes, the baseline tilt angle of the module is generally established in direct correlation with the geographical latitude of the installation site.

The specific geometric relationship between the incoming solar radiation and the receiving surface of the panel is quantitatively defined as the angle of incidence (designated as α). Peak electrical generation is attained when this solar irradiance strikes the panel's surface perfectly perpendicularly during solar noon. Consequently, establishing an exact 90° angle of incidence relative to the incoming solar rays constitutes the theoretical optimum for maximizing energy production. [8]

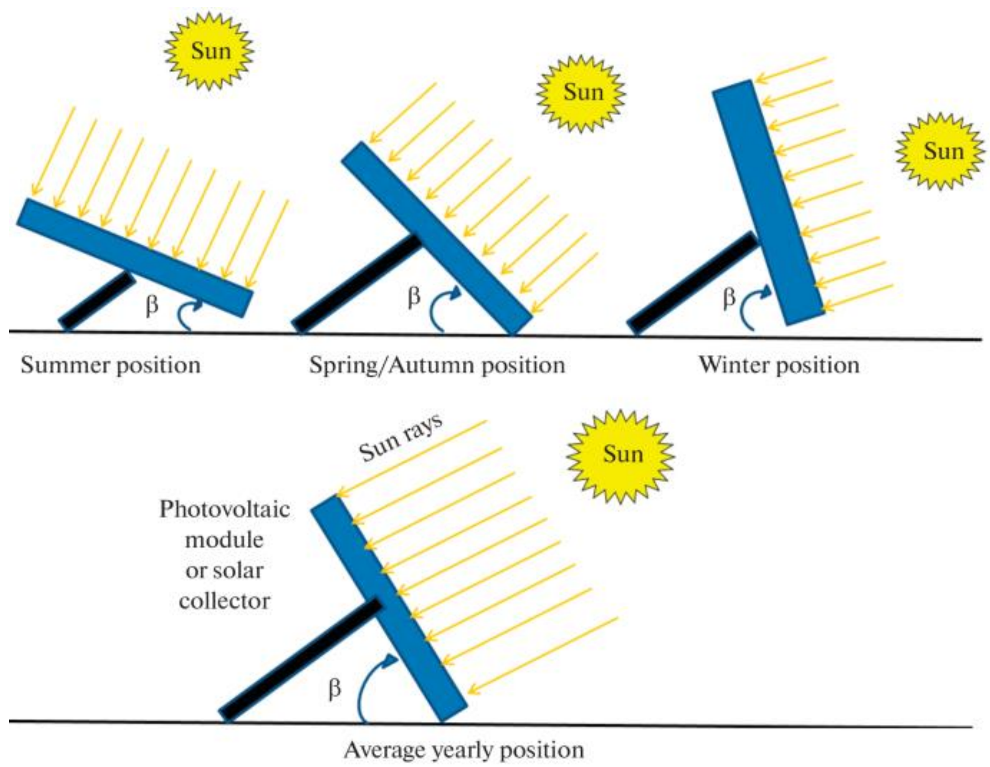


***Figure 1.20: Tilt of solar panel. [8]***

### 1.14.3. Architectures of Solar Installations :

A complete photovoltaic installation comprises several specialized components that operate in tandem to generate, manage, and store energy:

- **Photovoltaic Panels:** These arrays serve as the primary generators, synthesizing direct current (DC) electrical power from incident solar radiation.
- **Charge Regulator (Controller):** This device systematically governs the charging and discharging cycles of the battery bank, optimizing energy transfer based on battery capacity while enforcing critical electrical safeguards.

- **Inverter:** This component is responsible for the crucial inversion of direct current into alternating current (AC), ensuring compatibility with conventional AC-powered loads and receivers.
- **Battery Storage:** These accumulators harvest and store surplus electrical energy generated during daylight hours, guaranteeing uninterrupted power availability during nocturnal periods or suboptimal meteorological conditions.
- **DC Receivers:** Purpose-built direct current appliances can be integrated directly into the system circuit. The utilization of such devices is noted to be highly energy-efficient and economically advantageous. [8]

**1.14.3.1. Regulator Interconnection Protocol :**

Following the strategic physical placement of the battery bank, charge controller, and solar arrays, taking into account optimal cable lengths and requisite installation clearances, the components must be systematically wired to the regulator. Subsequent to establishing a secure grounding connection, the integration sequence must strictly adhere to the following order: [8]

**a. Battery Integration**

1. Initiate the procedure by disengaging the protective fuse located on the positive (+) cable.
2. Secure the conductors to the charge controller by attaching the red cable to the positive (+) terminal and the black cable to the negative (-) terminal.
3. Terminate the opposing ends of these cables at the corresponding poles of the battery bank (red conductor to the positive terminal, black conductor to the negative terminal), ensuring the connections align with the established parallel wiring schematic.

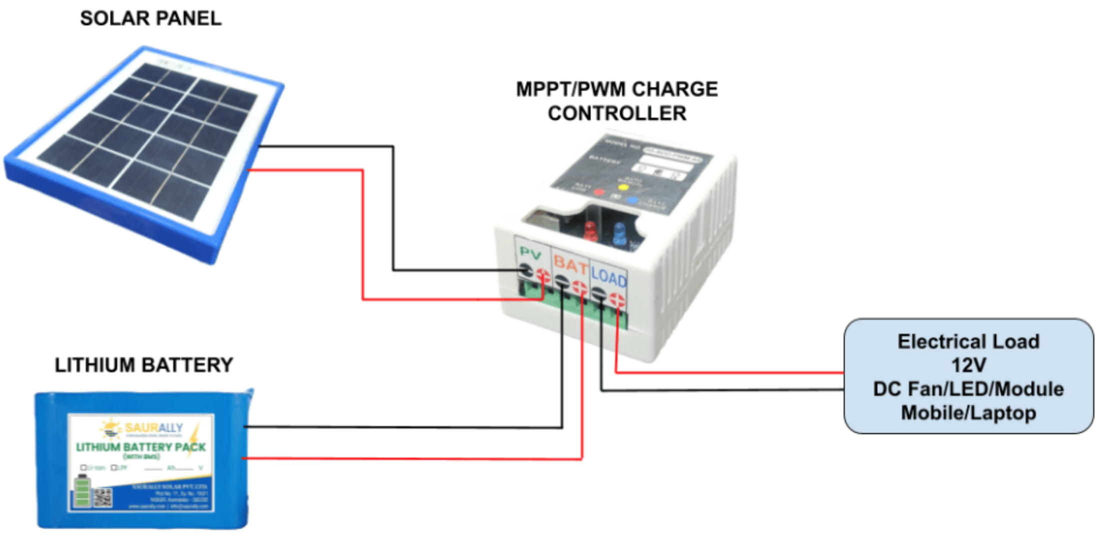


***Figure 1.21: Connection to the regulator.***

**b. Photovoltaic Panel Integration**

1. Initially, obscure the solar array with an opaque protective cover to temporarily halt the generation of electrical current.
2. Connect the corresponding wiring to the panel's output terminals, ensuring strict adherence to proper polarity (e.g., connecting the red conductor to the positive terminal and the black conductor to the designated negative terminal, which may occasionally be color-coded blue depending on regional standards).
3. Terminate the opposite ends of these conductors at the respective positive (+) and negative (-) input terminals on the charge regulator.

**c. Load (Consumer) Connection**

The synthesized electrical energy is subsequently distributed to power one or multiple terminal appliances, such as illumination systems, refrigeration units, or water pumps. The connection sequence is as follows:

1. Verify that all consumer appliances are switched to the "OFF" position.

2. Route and connect the conductors from the primary distribution panel to the designated load terminals on the regulator.
3. Systematically verify all electrical polarities and inspect the mechanical integrity of the connections.
4. Reinstall the protective fuse on the battery circuit and integrate any applicable fuses on the regulator.
5. Remove the opaque protective cover from the solar panel to initiate power generation.
6. Sequentially activate the consumer loads.

#### 1.14.4. Lightning Protection and Grounding Protocols

##### 1.14.4.1. Lightning and Surge Protection

The integration of a surge protection device (SPD) is imperative to safeguard the electrical infrastructure against high-voltage transients. Positioned inline between the photovoltaic array's fusing and the charge regulator, the SPD must be bonded to the earth grounding system. This configuration ensures the safe dissipation of localized lightning strikes or static accumulations, which are frequently attracted by the metallic racking structures of the solar modules. In

systems interfacing with an alternating current (AC) local grid, a supplementary AC surge protector should also be installed at the primary service entrance of the facility.

##### 1.14.4.2. Grounding (Earthing) Systems

A comprehensive grounding network is mandatory to guarantee the safety of both operating personnel and sensitive electronic equipment. Consequently, the metallic support structures of the PV modules, all surge arresters, and the inverter chassis must be securely and electrically bonded to a common earth ground [8].

### 1.15. Electrical Characteristics of a Photovoltaic Generator

#### 1.15.1. Current-Voltage (I-V) Characteristics

The fundamental current-voltage (I-V) curve of a photovoltaic device is derived from the empirical relationship between the voltage, current, and resulting power output of a specific solar cell, module, or comprehensive array. These graphical representations supply critical diagnostic data regarding the system's dynamic electrical behavior and its maximum capacity for power generation.

It is crucial to note that equipment manufacturers consistently baseline these operational parameters and their corresponding I-V profiles against Standard Test Conditions (STC). As universally defined, STC parameters consist of an incident solar irradiance of 1000 W/m², an internal cell operating temperature of 25°C, and an Air Mass (AM) spectral distribution of 1.5 [9].

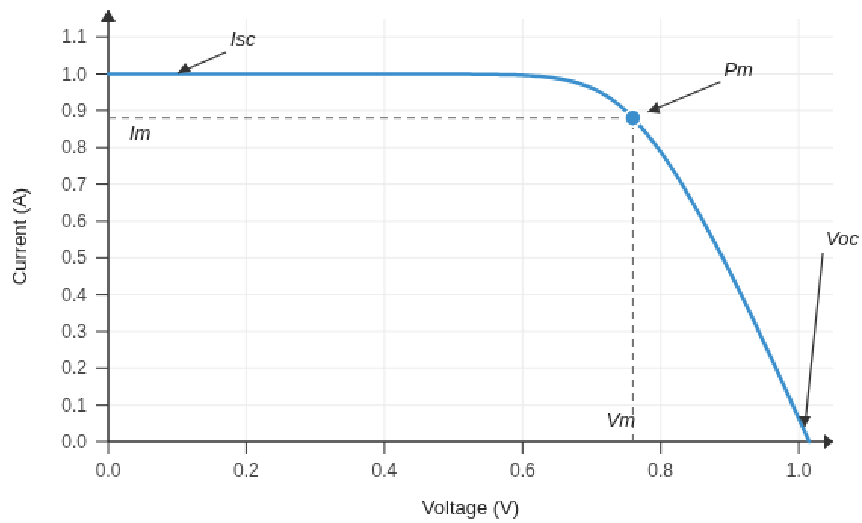


***Figure 1.22: I-V characteristic curve.***

### 1.15.2. Photovoltaic Cell Parameters

The fundamental parameters utilized to characterize a photovoltaic cell include [10]:

**a. Open-Circuit Voltage ($V_{OC}$):**

The open-circuit voltage represents the absolute maximum electrical potential a solar cell is capable of producing. This specific condition occurs when the external circuit is completely open, meaning no current is actively flowing through it. In this state, $V_{OC}$ corresponds to the forward bias voltage where the cell's internal dark current density perfectly balances out the photo-generated current density. Because it is intrinsically linked to the photo-generated current density, the value of $V_{OC}$ can be mathematically derived from Equation (1.2) by establishing that the net current is equal to zero.

$$V_{OV} = \frac{nkT}{q} \ln\left(\frac{I_{ph}}{I_0} + 1\right) \quad (1.2)$$

**b. Short-Circuit Current ($I_{SC}$) :**

The short-circuit current represents the absolute maximum electrical current that a solar cell is capable of generating. This peak value is attained specifically under conditions where the external circuit possesses zero resistance (no load), which consequently results in an electrical potential (voltage) of zero across the cell's terminals.

$$I_{SC} = \frac{I_{ph}}{1+\frac{R_S}{R_{sh}}} \quad (1.3)$$

**C.Maximum Power Point:**

The maximum power point represents the absolute peak electrical power that a solar cell is capable of generating under specific operating conditions. This value is determined by the product of the maximum current ($I_{mp}$) and the corresponding maximum voltage ($V_{mp}$), which graphically corresponds to a specific area as demonstrated in Equation (I.4).

$$P_{mp} = I_{mp}.V_{mp} \quad (1.4)$$

**d. Fill Factor (FF):**

The Fill Factor is defined as the specific ratio between the actual maximum power (MP) produced by the solar cell and the calculated product of its open-circuit voltage ($V_{oc}$) and short-circuit current ($I_{SC}$).

$$FF = \frac{Power\ at\ mpp}{Theoritical\ maximum\ power} = \frac{I_{mp}.V_{mp}}{I_{SC}.V_{OC}} \quad (1.5)$$

**e. Conversion Efficiency (η):**

Integrating a solar cell into an electrical circuit results in the conversion and subsequent collection of a specific percentage of available power. This performance metric is designated as the conversion efficiency (η) of the device. The quantitative calculation of this efficiency is derived by establishing a ratio: the maximum power point ($P_{max}$) divided by the product of the incoming solar irradiance (G, expressed in W/m²) under standard test conditions (STC) and the effective surface area of the solar cell ($A_c$, expressed in m²) [11].

$$\eta = \left(\frac{P_m}{P_i}\right) = \frac{I_m . V_m}{P_i} = \frac{I_{SC} . V_{OC}}{P_i} * FF \quad (1.6)$$

**Pi :** incident light power

**Pm :** the maximum power converted into electricity.

### 1.16. Influence of Irradiance and Temperature :

#### 1.16.1. The Effect of Solar Irradiance

Over the course of a typical day, the levels of solar irradiance experience significantly greater fluctuations compared to ambient temperature changes. This variance in solar radiation exerts a profound impact on the overall efficiency of photovoltaic cells. As illustrated in Figure 1.23, there is a direct, proportional correlation between the amount of solar radiation absorbed by the cell and the magnitude of the electrical current it generates.

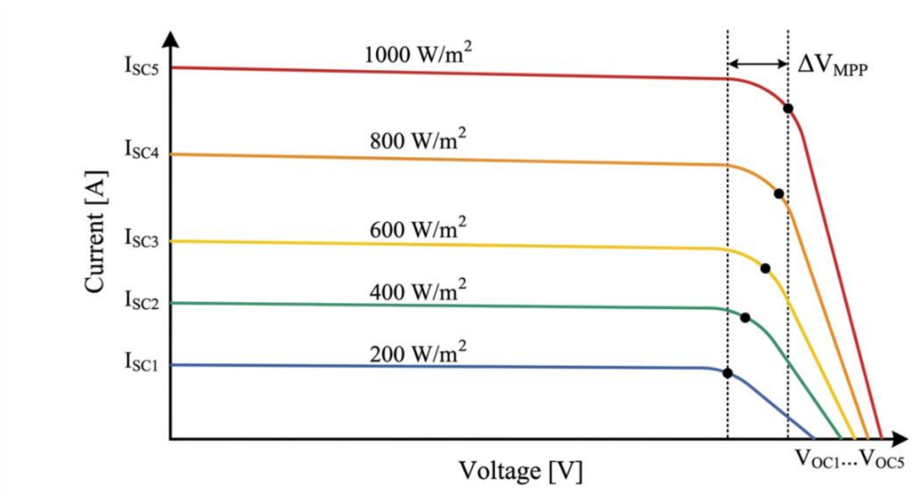


***Figure 1.23: I–V Characteristic curve of a PV module.[12]***

### I.16.2. The Effect of Temperature

As illustrated in Figure 1.24, temperature variations exert a significant influence on the electrical voltage of a photovoltaic panel. Utilizing the previously referenced PV panel as an example, the maximum power point voltage $V_{mpp}$decreases by approximately 10 V during hot summer conditions. Conversely, during colder winter days, this value typically increases by roughly 10 V compared to its baseline rating under Standard Test Conditions (STC). In contrast to these notable voltage fluctuations, the overall electrical current produced by the PV system experiences only a marginal increase in response to rising temperatures.

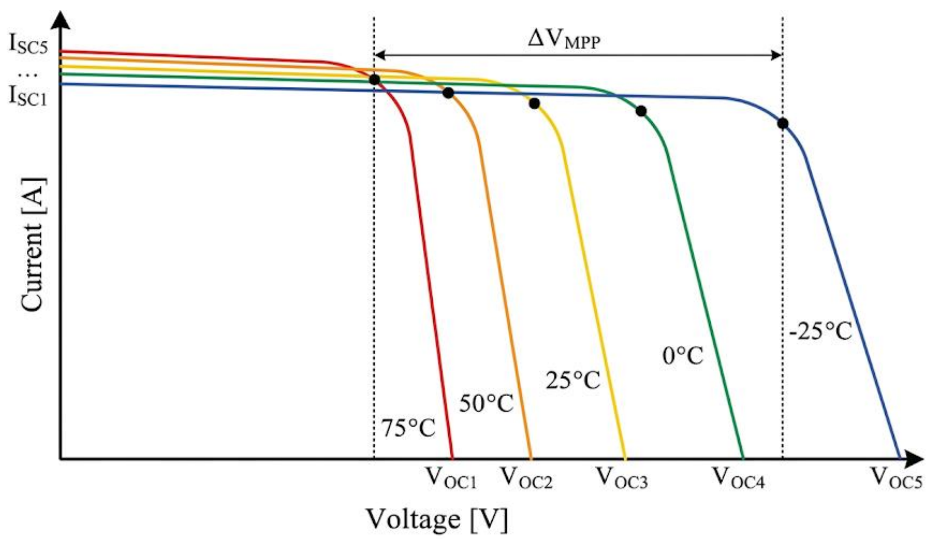


***Figure 1.24: I–V Characteristic Curve of a PV Module at Constant Received Solar Radiation and Variable Temperature.[12]***

### 1.17. The Photovoltaic Generator

A photovoltaic generator system is comprised of multiple interconnected modules, accompanied by an assortment of integral components that collectively facilitate the generation and subsequent conversion of energy.

*Figure 1.25: Photovoltaic generator.*

### 1.17.1. Energy Storage (Battery) :

The electrical storage capacity of a battery is universally quantified in ampere-hours (Ah). Within the context of photovoltaic systems, lead-acid batteries represent the most frequently deployed storage technology. However, for specialized applications operating under extreme climatic conditions, nickel-cadmium batteries are occasionally utilized as a robust alternative, despite their notably higher associated costs [13].

### 1.17.2. Charge Regulators :

Charge regulators function as the critical management interface interconnecting the PV modules, the battery bank, and the active electrical load. Their essential purpose is to shield the battery from potentially damaging overcharging or severe depletion by strictly governing the flow of both incoming and outgoing electrical currents.

### 1.17.3. Inverters :

The primary operational duties of the inverter consist of transforming direct current (DC) electricity into alternating current (AC), precisely shaping the waveform of the synthesized AC output, and actively regulating the effective (RMS) value of the delivered voltage.

### 1.17.4. Load :

The various appliances, illumination networks, and general equipment drawing power from the solar installation collectively form the electrical load of the PV system. The integration of highly energy-efficient load devices directly improves the overarching efficiency and economic performance of the entire system.

## 1.18. Applications of Photovoltaic Systems :

The primary applications of photovoltaic technology are organized into several distinct structural configurations based on their intended operational environment.

### 1.18.1. Autonomous Photovoltaic Installations :

The fundamental purpose of an autonomous (off-grid) system is to reliably supply power to one or multiple consumer loads situated in remote zones completely isolated from the centralized electrical grid. As illustrated in Figure 1.26, the deployed photovoltaic field is capable of directly synthesizing the necessary electrical energy to power various receivers, including standard lighting circuits and domestic household equipment [10].

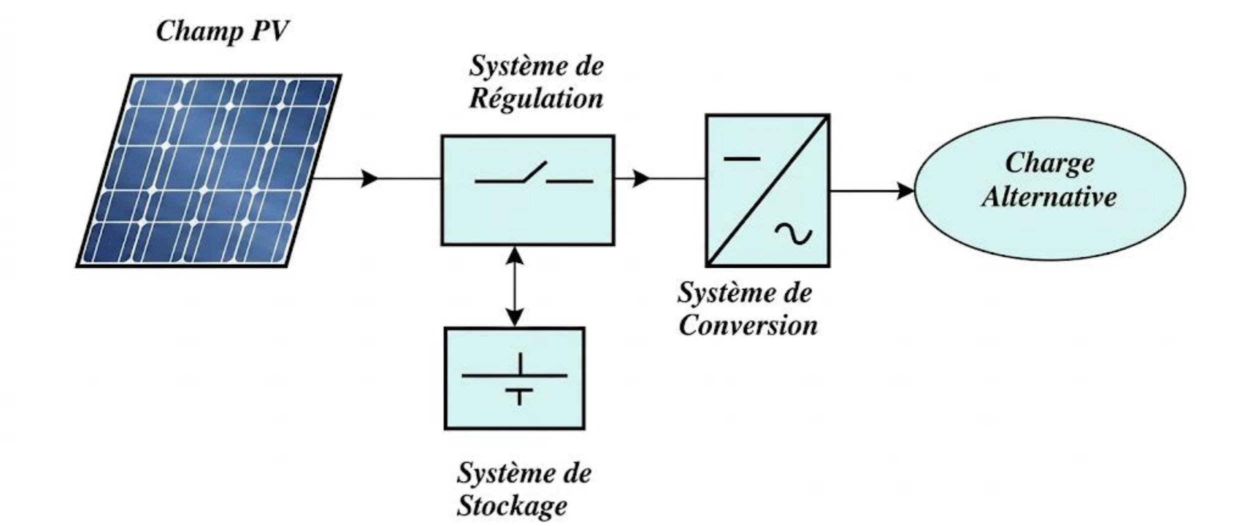


***Figure 1.26: Simplified diagram of an autonomous photovoltaic installation*[23]**

### 1.18.2. Grid-Connected Photovoltaic Systems :

These specific architectures are deployed at sites that already maintain an active connection to the centralized electrical grid. They are predominantly installed on residential properties or commercial facilities that receive adequate solar exposure and intend to utilize a renewable energy source.

A defining characteristic of a grid-connected photovoltaic generator is that it fundamentally negates the requirement for localized energy storage. Consequently, this configuration effectively eliminates the battery bank, which is generally considered the most problematic and expensive component of a solar installation.

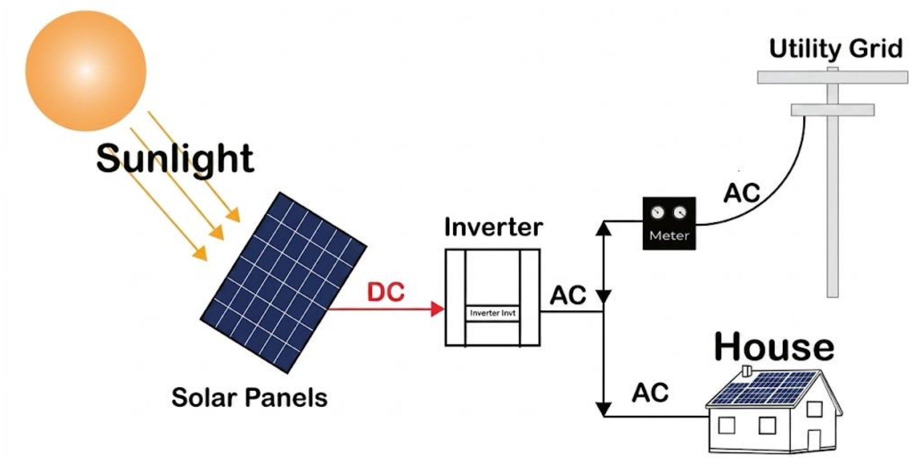


*Figure 1.27: Grid-Connected Photovoltaic Systems*

### 1.18.3. Hybrid Photovoltaic Systems :

Hybrid photovoltaic systems are integrated architectures that combine the primary solar array with one or more supplementary energy generation sources, such as wind turbines, diesel generators, or cogeneration plants. This specific type of multi-source installation is strategically deployed in scenarios where the standalone photovoltaic generator is insufficient to fully satisfy the total required energy demand [13].

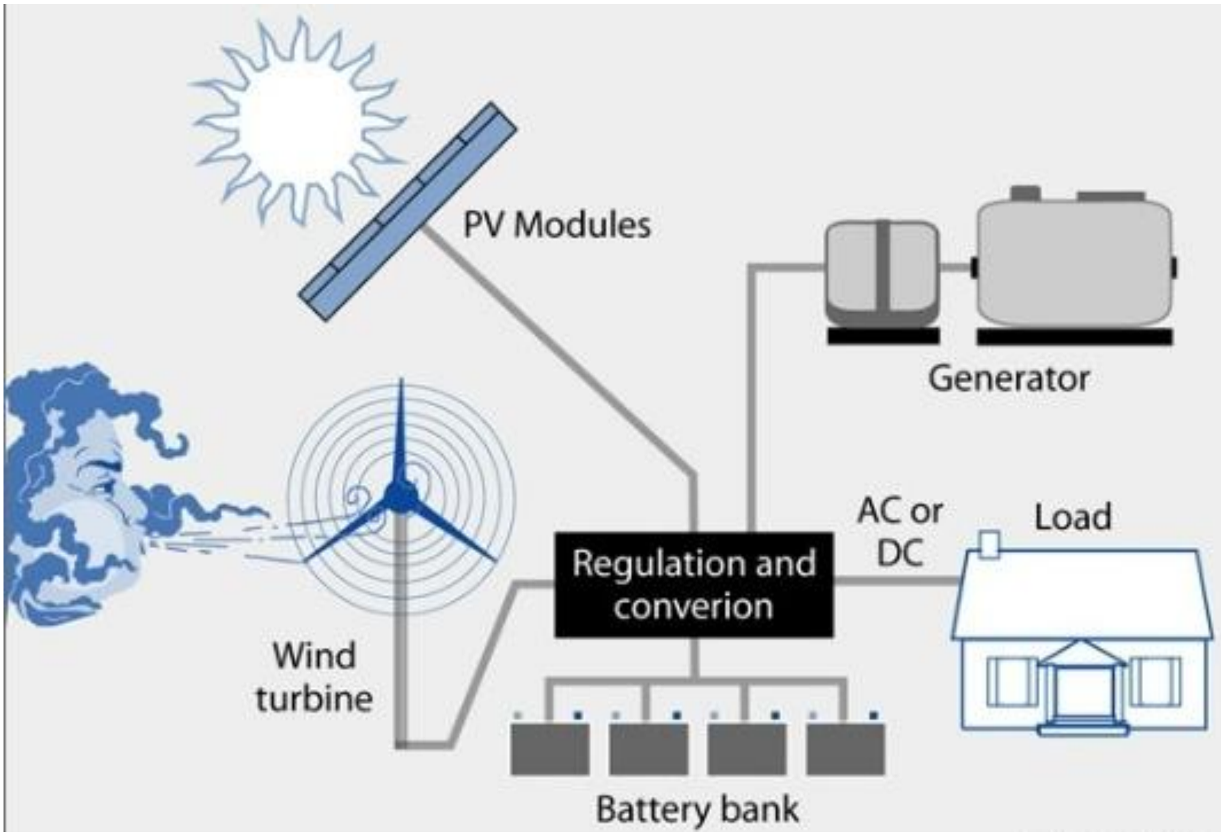


*Figure 1.28: Hybrid photovoltaic systems*

## 1.19. Advantages and Disadvantages of Photovoltaic (PV) Energy

### 1.19.1. Advantages

- **Exceptional Reliability:** Most manufacturers guarantee PV modules for up to 25 years.
- **Mechanical Simplicity:** The complete absence of moving parts makes PV systems highly reliable and particularly well-suited for isolated regions, which also justifies their widespread utilization in spacecraft.
- **Scalability:** The inherently modular nature of photovoltaic panels allows for simple adaptation to diverse energy requirements. Systems can be precisely sized to power applications ranging from mere milliwatts up to multi-megawatt installations.
- **Low Operational Expenses:** Operating costs are remarkably low due to minimal maintenance requirements. Furthermore, PV systems do not necessitate fuel consumption, logistical transportation, or highly specialized operational personnel.

- **Environmental Benefits:** Photovoltaic technology possesses strong ecological qualities; the energy generation process is entirely non-polluting, silent, and produces very little waste.

### 1.19.2. Disadvantages:

- **High Initial Investment:** The manufacturing of photovoltaic modules involves advanced, high-technology processes that require substantial capital investments.
- **Space Requirements:** Large-scale energy installations demand a significant footprint and land occupation.
- **Efficiency Limitations:** The practical conversion efficiency of a standard module remains relatively low (notably, the theoretical efficiency limit for a crystalline silicon cell is capped at 28%).
- **Economic Competitiveness:** Currently, photovoltaic generators are primarily competitive with traditional diesel generators only in scenarios involving low energy demands within isolated geographic areas.
- **Storage Costs:** When the chemical storage of electrical energy (via batteries) becomes necessary, the overall cost of the PV system increases significantly. While the overarching reliability and performance of the system can remain equivalent, this is strictly contingent upon the careful and correct selection of the battery bank and its associated regulatory components.

## 1.20. Photovoltaic Water Pumping Systems:

Securing a reliable water supply represents a highly common challenge for remote locations and isolated communities situated far from natural waterways and centralized electricity grids. To guarantee water access in these areas, the implementation of a standalone power source is essential, with photovoltaic solar energy serving as one of the most prevalent solutions. The integration of these technologies creates a "Photovoltaic Water Pumping System," as illustrated in Figure I.29.

The fundamental objective of this system is to resolve water scarcity issues by efficiently extracting and pumping water from local wells, even in highly rural environments. These photovoltaic water pumping architectures can be deployed across a multitude of domains, including residential water supply, agricultural operations (such as irrigation, livestock breeding, and general agriculture), water purification facilities, and firefighting infrastructure. Functionally, this setup combines two principal subsystems: the solar photovoltaic generator and the mechanical water pumping apparatus.

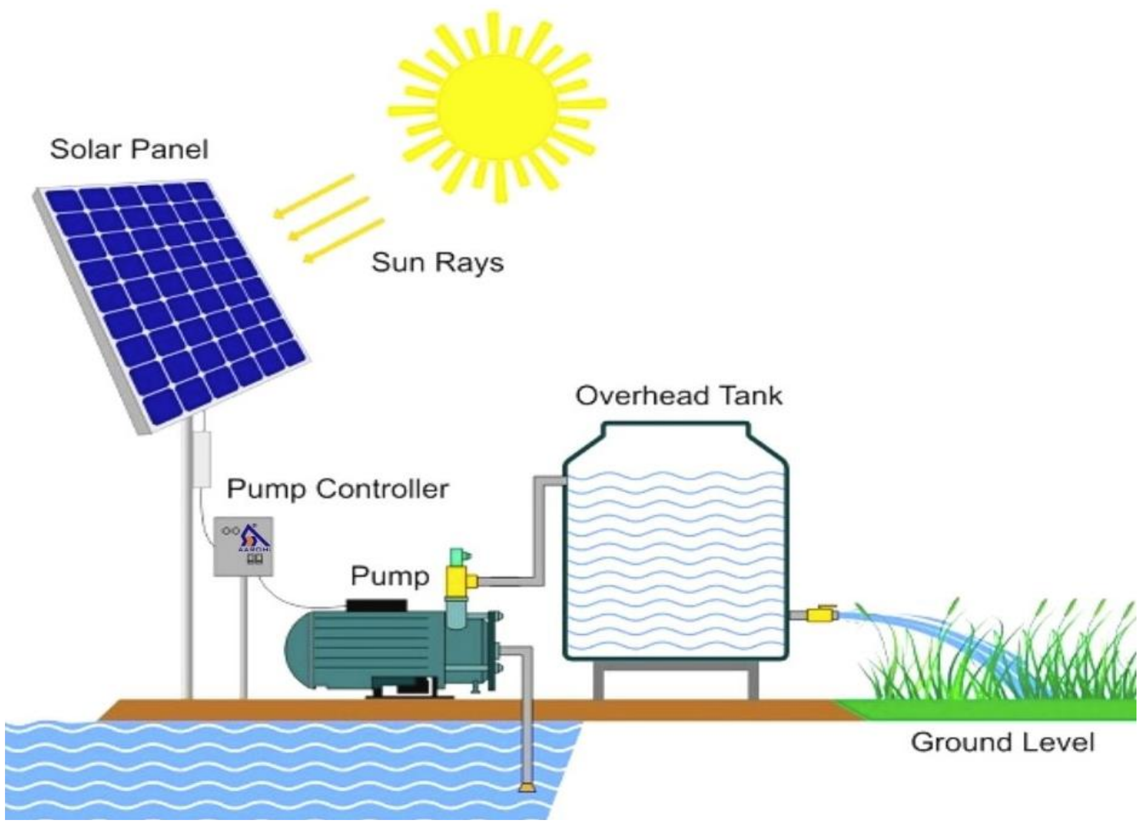


*Figure 1.29: Photovoltaic Water Pumping System*

### 1.20.1. Selection of Solar Pumping Systems

Solar pumps have become a highly favored solution for small-scale drinking water supply networks. Historically, rural pumping stations relied heavily on diesel generators to meet their electrical demands. However, operating diesel engines necessitates extensive maintenance, including frequent filter replacements, refueling, and oil drains.

In stark contrast, solar pumps demand minimal oversight. Certain models can operate autonomously for up to five years without requiring direct mechanical intervention. Their daily operation is entirely automatic, functioning in tandem with the sun's trajectory. Consequently, this solution is exceptionally well-suited for remote applications where monitoring and supplying a traditional diesel system would be logistically challenging [8]. Overall, solar pumping effectively fulfills a vast majority of water needs, including:

- Domestic use
- Provision of drinking water
- Livestock watering
- Agricultural irrigation

### 1.20.2. Types of Solar Pumping Configurations

#### 1.20.2.1. Direct Pumping (Pumping "Over the Sun")

Direct solar pumping yields a straightforward, highly reliable, and cost-effective photovoltaic setup. In this configuration, water is actively pumped during daylight hours and accumulated directly within a physical storage tank. This method, referred to as hydraulic storage, allows the reserved water to be distributed later as demand dictates, entirely eliminating the need for electrical batteries.

#### 1.20.2.2. Indirect Pumping (Pumping with Energy Storage)

In an indirect architecture, the electrical energy generated by the solar panels is stored within battery banks rather than being immediately used to move water. This allows pumping operations to occur on-demand, even during the night or in the absence of sunlight. However, this system incurs higher capital and operational costs compared to direct pumping, primarily due to the necessity of periodically replacing the batteries, which inherently possess a relatively short operational lifespan [9].

### 1.20.3. Components of a Photovoltaic Pumping System

A standard solar pumping installation is generally comprised of the following key sub-systems [10]:

- **The Photovoltaic Generator (PVG):** The solar array responsible for power generation.
- **The Electric Pump Group:** The mechanical hardware that moves the water.

- **Command and Control Electronics:** The regulating interface that manages power delivery.
- **The Storage Unit:** Either a physical water tank (hydraulic storage) or a battery bank (electrical storage).

### 1.20.4. The Electric Pump Set

#### 1.20.4.1. Pump Fundamentals

A pump is a mechanical device engineered to transport fluids (liquids or gases) or slurries through aspiration and repression mechanisms. Pumps are broadly categorized into two primary classifications: centrifugal pumps and positive displacement pumps. Positive displacement variants are particularly adapted for elevating low fluid flow rates against high system pressures.

#### 1.20.4.2. Centrifugal Pumps

Centrifugal water pumps leverage centrifugal force to pressurize and propel water from the intake (inlet) to the discharge (outlet). This dynamic process is achieved via a rotating assembly of vanes, known as an impeller, which is driven by a central pump shaft.

As water is drawn into the impeller, the rotational kinetic energy is transferred to the fluid. The applied centrifugal force rapidly accelerates and pressurizes the water, flinging it outward from the impeller's center. A surrounding spiral-shaped casing, called a volute, subsequently catches and channels this newly pressurized water toward the designated outlet.

*(Note regarding the text: The structural rotation is typically observed as clockwise when viewed directly from the motor mount) [9]*.

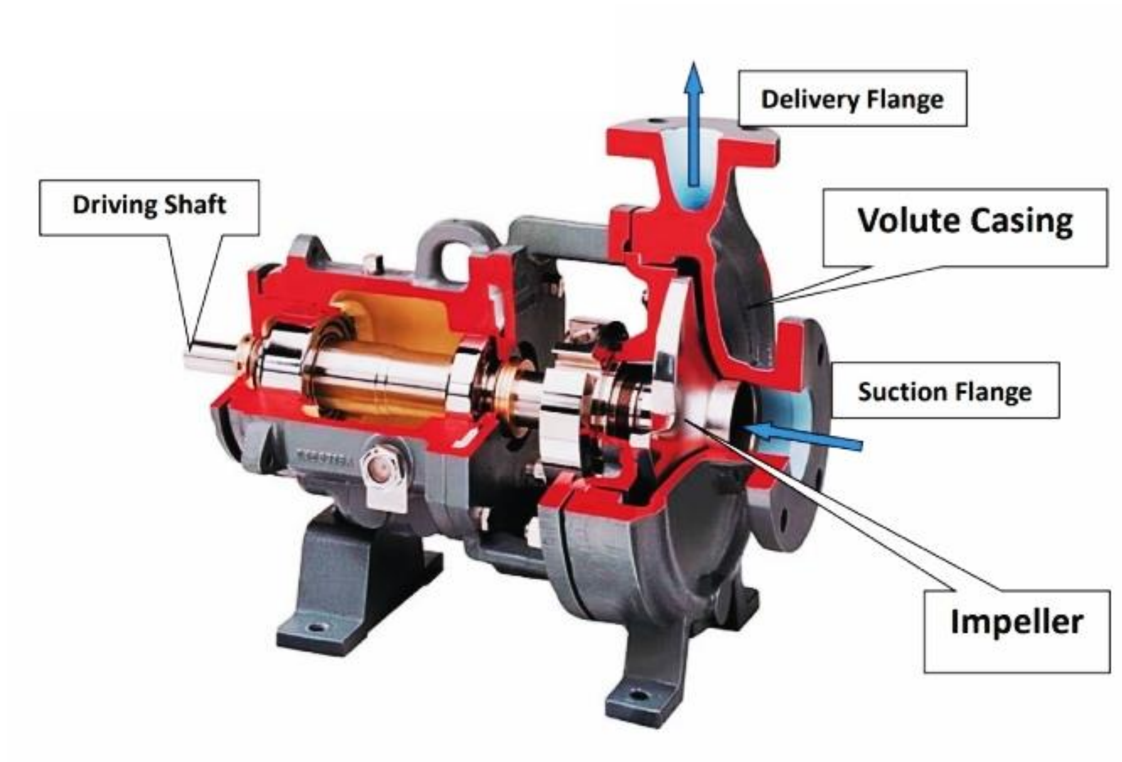


***Figure 1.30: Centrifugal Pump.***

For the designated Solar Water Pumping System (SWPS), a dynamic centrifugal pump was chosen. This specific selection is justified by its lower maintenance demands and its superior capability to synchronize with the electrical power output provided by the photovoltaic generators.

The mechanical torque demanded by the pump maintains a direct proportionality to the square of its rotational rotor speed, which is expressed by the following equation:

$$T_L = K_p \Omega_r^2 \quad (1.7)$$

Within this formula, $K_p$represents the constant of proportionality, which is defined as:

$$K_p = \frac{P_{np}}{\Omega_{rn}^3} \quad (1.8)$$

The resulting water flow rate and the operational pressure delivered by the pump are fundamentally dictated by the total system head and the mechanical power effectively available at the spinning impeller. To streamline the calculation of these output parameters, one can utilize the affinity laws. These rules simplify the process by requiring only the pump's baseline ratings alongside actual input variables, specifically the applied torque and rotor speed [13].

**a. The Affinity Laws**

Standard pumping processes necessitate that specific hydraulic criteria, namely, fluid head and flow rate, are properly satisfied. The Affinity Laws provide established mathematical correlations utilized to forecast how a pump's performance curves will shift in response to modifications in either the physical diameter of the impeller or the rotational shaft speed (N).

Assuming the impeller diameter remains fixed, the Affinity Laws establish that for any specific pump, the performance metrics will vary according to the following relationships relative to rotational speed [14]:

- **Flow Rate (Q):** Will be directly proportional to the shaft speed.
- **Head (H):** Will be directly proportional to the square of the shaft speed.
- **Required Power (P):** Will be directly proportional to the cube of the shaft speed.

$$\frac{Q_1}{Q_2} = \frac{N_1}{N_2} \quad (1.9)$$

$$\frac{H_1}{H_2} = \left(\frac{N_1}{N_2}\right)^2 \quad (1.10)$$

$$\frac{P_1}{P_2} = \left(\frac{N_1}{N_2}\right)^3 \quad (1.11)$$

### 1.20.4.3. Advantages of Centrifugal Pumps :

The selection and use of centrifugal pumps offer several distinct operational benefits:

- **Mechanical Simplicity:** These pumps operate without the need for internal valves and feature a very limited number of moving components. This streamlined design facilitates manufacturing using a wide variety of materials and allows the equipment to operate at high rotational speeds while requiring minimal ongoing maintenance.
- **Consistent Performance and Compact Design:** Centrifugal pumps deliver a highly stable and uniform fluid output. Furthermore, they boast a notably compact physical footprint, occupying significantly less space than alternative pump designs capable of generating an equivalent power output.
- **High Capacity:** These systems are exceptionally well-suited for processing and transferring substantial volumes of water.

## 1.21. Conclusion :

This chapter has provided a comprehensive overview of the foundational principles of photovoltaic systems, detailing their essential components and primary architectural classifications. Additionally, it explored the core operational concepts of solar cells, encompassing their mathematical modeling, key performance assessment parameters, and characteristic curves. Through the analysis of these specific curves, the direct operational impacts exerted by fluctuating ambient temperatures and varying levels of solar irradiance were effectively visualized and evaluated.

# Chapter 2

# MODELING OF SOLAR PUMP BASED ON SYNRM MACHINE

## 2.1. Introduction :

Globally, water pumping has traditionally relied on conventional grid electricity or diesel generators. However, the ongoing depletion of these conventional energy sources and their detrimental environmental impacts have driven growing interest in renewable alternatives, such as solar-photovoltaic, solar-thermal, wind, and biomass energy. Optimizing the utilization of both water and energy resources has emerged as a critical global priority over the past decade and will only increase in importance in the future [14].

Currently, utilizing photovoltaic (PV) technology to power water pumps is a rapidly emerging field presenting significant technical opportunities. The shift toward solar PV is largely motivated by the continuous decline of oil reserves, uneven resource distribution, and the escalating costs of electricity—factors that are particularly concerning for developing nations. Consequently, Solar Photovoltaic Water Pumping Systems (SPVWPS) have seen enormous improvements in widespread acceptance, reliability, and overall performance for providing domestic, livestock, and irrigation water in remote locations. Beyond these benefits, SPVWPS are highly durable and capable of withstanding extreme weather conditions, including snow and ice. Most importantly, solar power is fundamentally well-suited for water pumping because the peak demand for water naturally aligns with the periods of highest solar irradiance [13].

Historically, DC motor-driven PV pumps have been widely deployed globally because they connect directly to the PV array and offer simple speed adjustment. Nevertheless, these systems are hindered by higher motor costs and significant maintenance requirements due to the presence of mechanical commutators and brushes [15]. To overcome these limitations, brushless motor architectures have emerged as a highly attractive alternative. While brushless permanent magnet DC motors have been successfully implemented [16], their application remains largely restricted to low-power PV systems.

Recent research has thoroughly investigated AC pumping systems driven by either current-source or voltage-source inverters [14]. For instance, Induction Motors (IMs) provide a robust, reliable, and practically maintenance-free alternative, characterized by their reduced unit cost and rugged, brushless rotor construction [17]. Similarly, Permanent Magnet Synchronous Motors (PMSMs)often referred to as brushless DC motorscoupled with centrifugal pumps have proven highly effective for PV water pumping applications [11].

Building upon these advancements, the Synchronous Reluctance Motor (SynRM) powered by a PV generator represents a highly promising brushless architecture that warrants thorough investigation. Despite its inherent advantages, the application of SynRMs within PV water pumping systems remains significantly underexplored in current academic literature to date [11].

**2.2. Modeling of System Components :**

This section details the development of MATLAB/Simulink models for the core components of the system. These models are constructed using the theoretical descriptions, electrical circuit topologies, and mathematical equations introduced throughout this chapter.

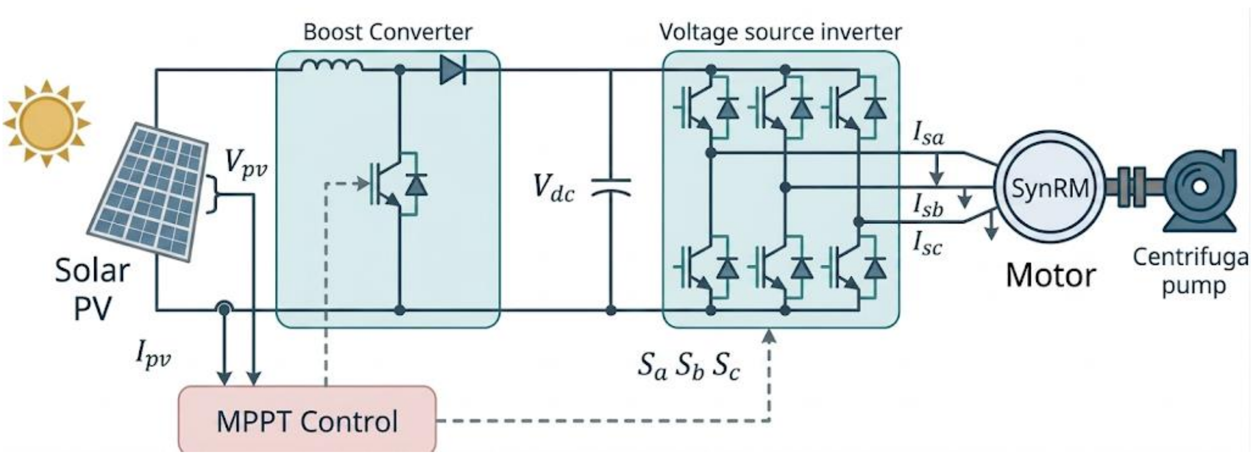


***Figure 2.1: Schematic diagram of the PV Water Pumping System***

**2.2.1. PV Array Modeling :**

The operational behavior of the PV array is characterized by the theoretical model presented in the following diagram. The electrical output of this array is a direct current (DC) that is directly proportional to solar irradiance levels, ambient temperature variations, and the structural arrangement of the interconnected modules per string.

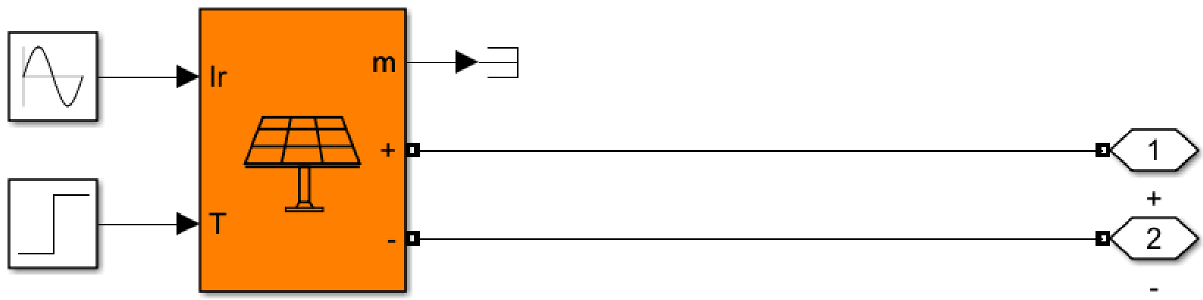


***Figure 2.2: PV panel model.***

The general current-voltage characteristic of a PV panel based on the single exponential model is:

$$I = I_{ph} - I_0\left(e^{\left(\frac{V+IR_s}{n_sV_t}\right)} - 1\right) - \left(\frac{V+IR_s}{R_{sh}}\right) \quad \textbf{(2.1)}$$

$$V_t = \frac{AkT_{stc}}{q} \quad \textbf{(2.2)}$$

## Where:

- Standard test conditions (A = 1000 W/m2; T = 25 °C; AM = 1.5)
- $I_{ph}$ The photo-generated current under Standard test conditions
- $I_0$ Dark saturation current under Standard test conditions
- $R_s$ , $R_{sh}$ Panel series resistance panel , parallel resistance
- $A$ diode quality factor

These constitute the five core parameters of the model. Furthermore, $K$ signifies Boltzmann's constant and $q$ indicates the elementary charge of an electron

The defining $I(V)$ relationship for this system is governed by the following equation:

$$I = I_{ph} - I_0 e^{\left(\frac{V+IR_S}{n_s V_t}\right)} - \frac{V+IR_S}{R_{sh}}\left(1 + \left(a\left(\frac{V+IR_S}{n_s V_{br}}\right)\right)^{-m}\right) \quad \textbf{(2.3)}$$

**Photovoltaic Module Inputs and Outputs :**

The simulated PV array requires two primary environmental inputs: ambient temperature and solar irradiance. Electrically, it delivers an output voltage across its positive and negative terminals. Furthermore, the module incorporates a data measurement bus (designated as output *m*), which multiplexes four critical parameters for continuous system monitoring:

- Photovoltaic voltage
- Photovoltaic current
- Input temperature
- Input irradiance

**Photovoltaic Module Identification:** For the simulation, a user-defined photovoltaic module with a maximum power rating of 326 W is configured using the Simscape library in MATLAB/Simulink 2020. The characteristics and parameters of the customized module are shown in the next table:

**Parameters of the User-Defined Photovoltaic Module :**

| | | | |
|---|---|---|---|
| *Maximum Power (W)* | 326.076 | *Cells per module (Ncell)* | 60 |
| *Open circuit voltage Voc (V)* | 39 | *Short-circuit current Isc (A)* | 10.1 |
| *Voltage at maximum power point Vmp (V)* | 34.8 | *Current at maximum power point Imp (A)* | 9.37 |
| *Temperature coefficient of Voc (%/deg.C)* | -0.36099 | *Temperature coefficient of Isc (%/deg.C)* | 0.102 |

***Table 2.1: PV panel characteristics***

The implemented PV model facilitates the generation of power-voltage (P-V) and current-voltage (I-V) characteristic curves, enabling a detailed analysis of the module's electrical response to varying environmental conditions. Specifically, to assess the direct impact of solar

radiation, the simulation evaluated the system across a range of irradiance levels from 200 W/m² to 1200 W/m², while the operating temperature was maintained at a constant 25°C.

**I-V and P-V curves for the PV array are shown in figure below:**

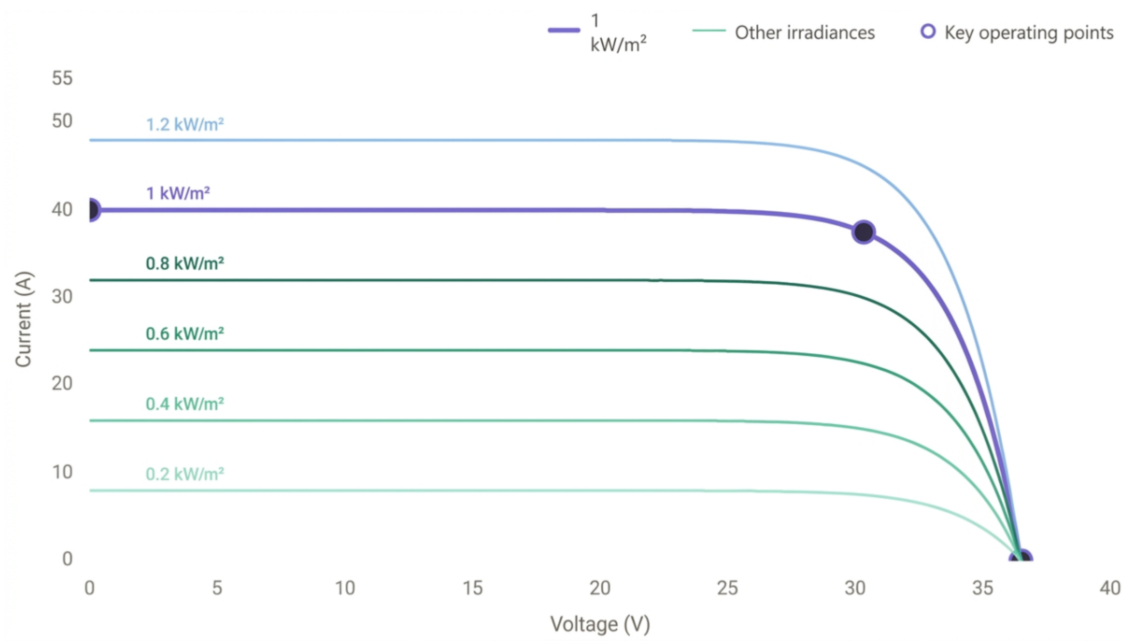


***Figure 2.3: PV array: I-V characteristic curve***

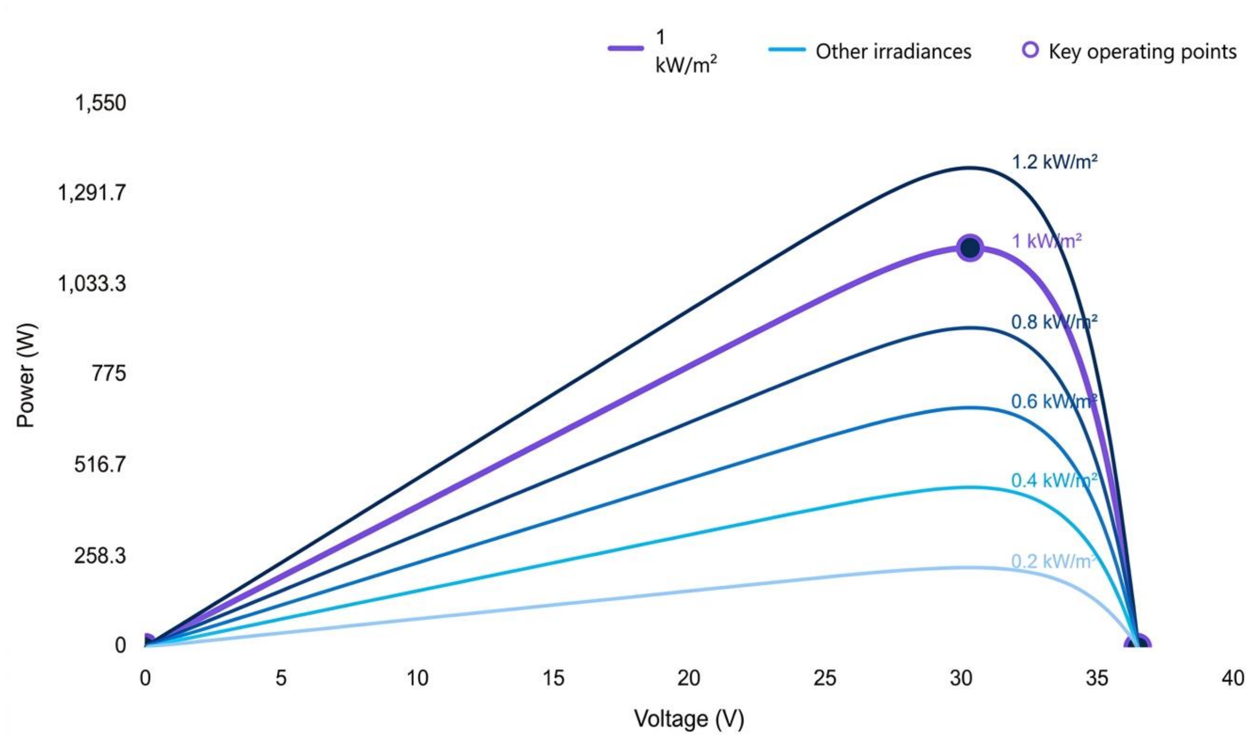


***Figure 2.4: PV array: P-V characteristic curve***

The resulting graphs clearly demonstrate that the panel's electrical characteristics are profoundly influenced by solar irradiance. The output current exhibits a high sensitivity to these fluctuations, maintaining a direct proportionality; as irradiance decreases, the generated current experiences a corresponding linear decline. Conversely, the voltage demonstrates greater stability, remaining relatively constant near its open-circuit value ($V_{oc}$) even as the current approaches zero.

Similarly, the power-voltage (P-V) characteristic curves preserve their fundamental shape across varying irradiance levels. However, consistent with the I-V characteristics, the total power output is directly dependent on the incident light. Consequently, the Maximum Power Point (MPP)—indicated by the plotted circlesdecreases systematically as irradiance drops. Furthermore, the graphs mathematically confirm that the open-circuit voltage ($V_{oc}$) represents the boundary condition where the total output power drops to zero.

### 2.2.2. Electrical Equivalent Circuit of the Photovoltaic Cell :

A review of existing literature reveals several established equivalent circuit models utilized to mathematically represent PV cells. Among these, the most widely adopted is the standard single-diode model, which incorporates both a series and a shunt resistance [17, 18]. As depicted in Figure 2.5, the fundamental photoelectric conversion is represented by a current source ($I_{ph}$), which generates a current directly proportional to the incident solar irradiation. Within this circuit topology, the series resistance accounts for the internal structural resistances of the cell, whereas the shunt resistance represents internal leakage currents.

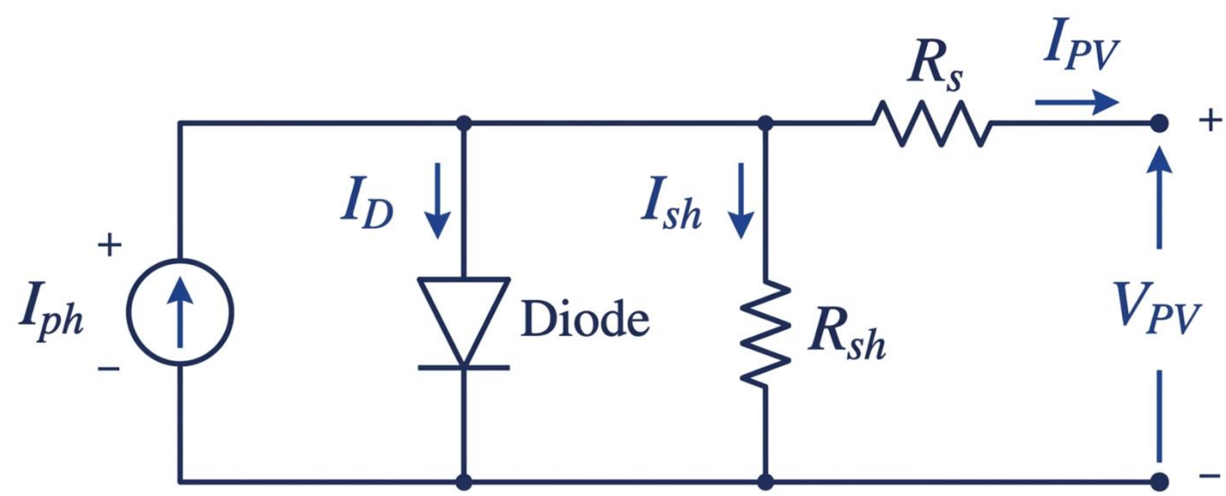


***Figure 2.5: The single diode model of PV cell***

The mathematical equation that expresses the PV cell is given in as follows:

$$I_{PV} = I_{ph} - I_D - \frac{V_D}{R_{sh}} \tag{2.4}$$

**Or :**

$$I_{PV} = I_{ph} - I_S\left[exp\left(\frac{q(V_{PV}+R_S I_{PV})}{AKT}\right) - 1\right] - \frac{V_{PV}+R_S I_{PV}}{R_{sh}} \tag{2.5}$$

**Where:**

- $I_{ph}$: is the light-generated current of the elementary solar cell (A).
- $I_D$: is the current of the parallel diode (A).
- $I_S$: is the reverse saturation current of the diode (A).
- $I_{PV}, V_{PV}$: are the output current (A) and voltage (V) of the PV cell, respectively.
- $\boldsymbol{q}$: is the elementary electron charge ($1.60217662 * 10^{-19} C$).
- $\boldsymbol{A}$: is the diode ideality factor, which depends on the specific PV cell technology.
- $\boldsymbol{K}$: is the Boltzmann constant ($1.38064852 * 10^{-23} J/K$).
- $\boldsymbol{T}$: is the temperature of the p-n junction in Kelvin (K).

## 2.3. Inverter-SynRMModeling:

### 2.3.1. Static DC-AC Converter:

A static converter is an electronic system designed to condition and regulate the electrical energy supplied to a specific receiver or load. The advent of modern power electronics in the mid-20th century enabled the development of these electrical power converters without the need for rotating mechanical components. The semiconductor technology underlying these devices is constantly evolving, offering several distinct advantages:

- Low manufacturing and operational costs.
- High power switching capabilities.
- Ease of integration and control.

**a. Definition of the Inverter :**

An inverter is a static power converter specifically designed to transform direct current (DC) power into alternating current (AC) power. By utilizing semiconductor switches, a constant DC input voltage can be alternately applied to the load terminals, effectively reversing the polarity.

By carefully sequencing the switching commands of these semiconductors, it is possible to generate an alternating output voltage with an average value of zero. Depending on the chosen control strategy، such as Pulse Width Modulation (PWM) or fundamental frequency switching (square wave control)، this output voltage may consist of one or multiple alternating pulse segments.

Inverters are generally classified based on several criteria:

- **By source type:** Voltage Source Inverters (VSI) and Current Source Inverters (CSI).
- **By number of phases:** Single-phase, three-phase, etc.
- **By number of output levels:** Two-level, three-level, multi-level, etc.

**b. Voltage Inverter Modeling:**

The three-phase voltage source inverter that powers the SynRM can be ideally represented by the standard inverter circuit diagram. The inverter consists of semiconductor switches (e.g., MOSFETs or IGBTs) denoted as $T_i$and $T_i'$(where $i = a, b, c$ corresponding to the three phases). The logical control signals associated with them are defined as $S_i$and $S_i'$, operating under the following complementary conditions:

- If $S_i = 1$, the upper switch $T_i$ is closed (conducting) and the lower switch $T_i'$is open.

- If $S_i$= 0, the upper switch $T_i$ is open and the lower switch $T_i'$ is closed (conducting).

In this standalone photovoltaic system, the inverter's input is directly supplied by the stabilized DC bus from the solar array. The machine-side converter (the three-phase voltage inverter) then transforms this DC power into the required alternating voltage to drive the SynRM.

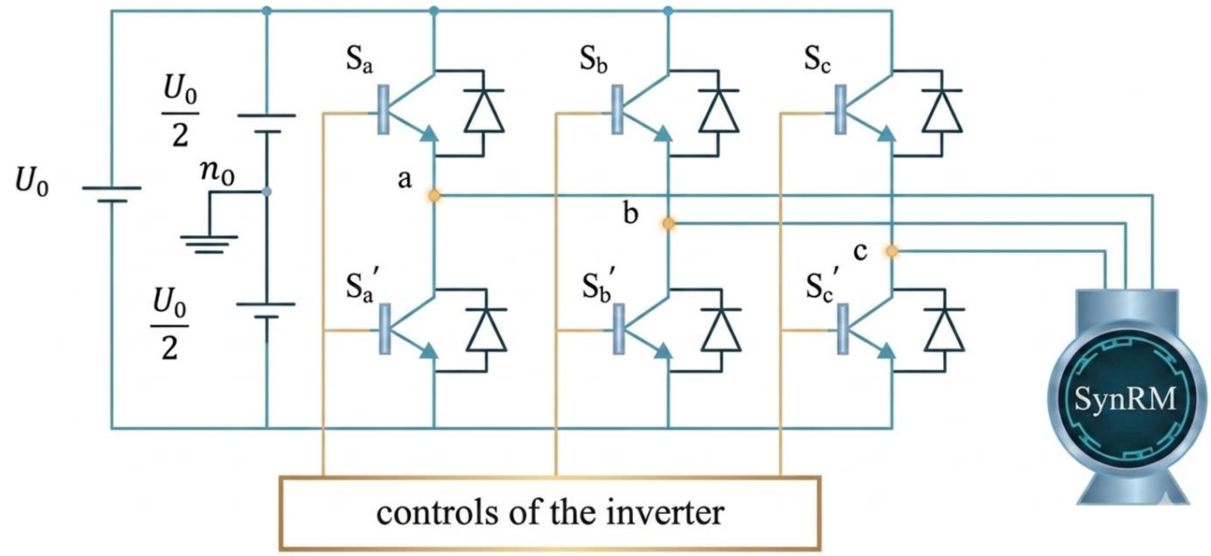


***Figure 2.6: Diagram of the SynRM – voltage inverter association***

For analytical modeling, the inverter's DC power supply is represented as an ideal source divided into two equal voltage components of $\frac{U_0}{2}$, connected at a fictitious neutral midpoint$n_0$. Each of the three inverter legs consists of two semiconductor switches operating in a complementary sequence. Free-wheeling diodes are connected in anti-parallel with the transistors to provide a safe path for inductive load currents. As illustrated in the equivalent circuit (Figure II.7), each leg of the inverter essentially functions as an ideal two-state switch.

Assuming the Synchronous Reluctance Machine (SynRM) features a balanced, star-connected stator winding, and $U_0$ represents the total DC link voltage feeding the inverter, the line-to-line voltages can be obtained directly from the inverter outputs [9]:

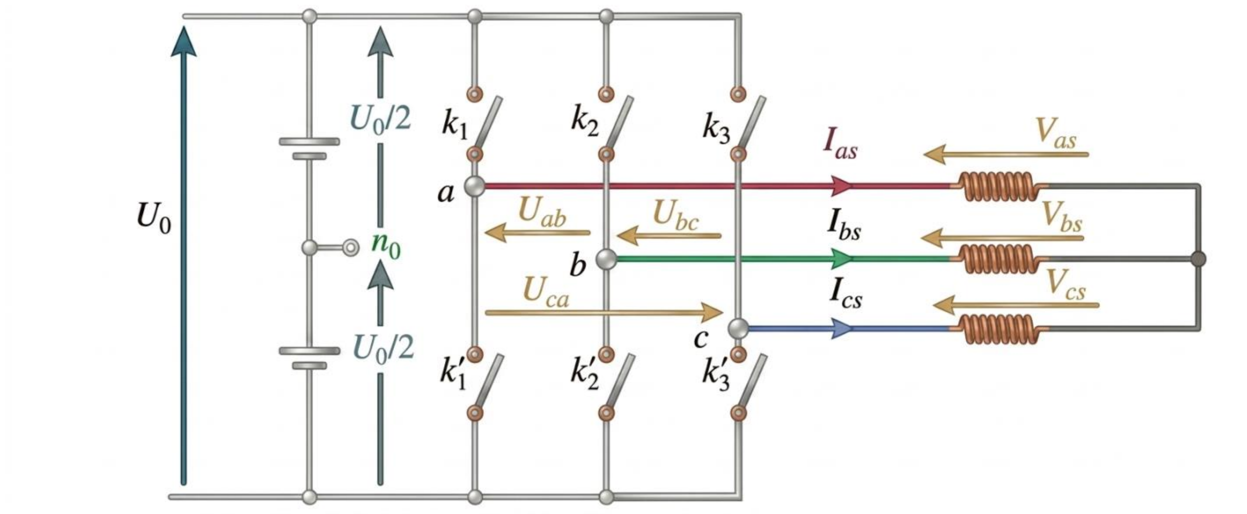


***Figure 2.7: Equivalent diagram of the inverter***

The line voltages delivered by the inverter are:

$$U_{ab} = Vas - Vbs = U0(Sa - Sb) \quad (2.6)$$

$$U_{bc} = Vbs - Vcs = U0(Sb - Sc) \quad (2.7)$$

$$U_{ca} = Vcs - Vas = U0(Sc - Sa) \quad (2.8)$$

The voltages Vas, Vbs and Vcs form a balanced three-phase voltage system then:

From (2.6) and (2.8) :

$$V_{as} = \frac{U_0}{3}(2S_a - S_b - S_c) \quad (2.9)$$

From (2.6) and (2.7) :

$$V_{bs} = \frac{U_0}{3}(2S_b - S_a - S_c) \quad (2.10)$$

From (2.9) and (2.10) :

$$V_{cs} = \frac{U_0}{3}(2S_c - S_a - S_b) \tag{2.11}$$

Therefore:

$$\begin{bmatrix} V_{as} \\ V_{bs} \\ V_{cs} \end{bmatrix} = \frac{1}{3}U_0 \begin{bmatrix} 2 & -1 & -1 \\ -1 & 2 & -1 \\ -1 & -1 & 2 \end{bmatrix} \begin{bmatrix} S_a \\ S_b \\ S_c \end{bmatrix} \tag{2.12}$$

### 2.3.2. SynRM Mathematical Model

The mathematical model of the SynRM is structurally comparable to that of a standard Induction Motor (IM). However, a primary distinction in the SynRM modeling is the assumption that rotor copper losses are negligible, as the SynRM rotor does not contain conductive windings or a squirrel cage.

The dynamic behavior of the SynRM, expressed in the synchronous $d - q$ rotor reference frame, is defined by the following stator voltage equations as in [23] :

$$V_d = R_s i_d - \omega_e L_q i_q + L_d \frac{di_d}{dt} \tag{2.13}$$

$$V_q = R_s i_q + \omega_e L_d i_d + L_q \frac{di_q}{dt} \tag{2.14}$$

where $v_d$and $v_q$ represent the terminal voltages along the direct and quadrature axes, respectively, while$i_d$ and $i_q$ denote the corresponding terminal currents along these axes.

$$T_e = \frac{3}{2}\mathrm{p}(L_d - L_q)i_d i_q \tag{2.15}$$

The mechanical dynamic equation governing the motor speed is expressed as:

$$T_e = J\frac{d\omega_m}{dt} + f\omega_m + T_L - T_K \quad (2.16)$$

Where $T_L$ denotes the applied load torque, $J$ is the total moment of inertia of the rotating mass, $\omega_m$ represents the mechanical angular velocity of the motor, $f$ is the viscous friction coefficient, $T_k$ accounts for the constant friction load, and $p$ signifies the number of pole pairs.

### 2.4. DC-DC Converter Modeling :

DC-DC static converters are essential power electronic interfaces used to condition the fluctuating DC voltage provided by the Photovoltaic (PV) array. This work specifically focuses on the implementation of a **Boost converter**.

In general, DC-DC converters can operate in either Continuous Conduction Mode (CCM) or Discontinuous Conduction Mode (DCM). In CCM, the inductor current flows continuously and never reaches zero during a switching cycle. In DCM, the inductor current drops to zero for a portion of the cycle. Because the dynamic frequency response of the power stage changes significantly between these two modes, the converter in this system is designed to operate strictly in CCM to ensure optimal stability and control performance across expected operating conditions.

#### 2.4.1. Boost Converter Modeling :

The Boost (step-up) converter is a fundamental non-isolated switched-mode power supply topology designed to elevate an input DC voltage to a strictly higher output DC voltage. In photovoltaic applications, it is frequently utilized to step up the variable PV array voltage to match the higher, stabilized DC-link voltage required by the inverter.

As illustrated in the electrical schematic (Figure 2.8), the power stage relies on a transistor acting as an active switch, driven by a Pulse Width Modulation (PWM) control signal. The fundamental operation and energy transfer of the converter can be described by two distinct topological states during a single switching period ($T_s$):

- **ON State (Switch Closed):** During the active phase of the duty cycle, the transistor is turned on. The inductor (L) is placed directly across the input voltage ($V_{in}$), causing the

- diode to become reverse-biased and isolating the output stage. Consequently, the inductor current ramps up linearly, effectively storing energy within its magnetic field.

- **OFF State (Switch Opened):** When the transistor is turned off, the inductor current cannot change instantaneously. The collapsing magnetic field reverses the inductor's voltage polarity, placing it in series with the input source. This forces the current through the now

- forward-biased diode, transferring the accumulated energy directly into the output capacitor and the load.

It is worth noting that even in the absence of active switching, the output capacitor will passively charge to the input voltage level ($V_{out}$ = $V_{in}$) via the forward-biased diode. However, under active high-frequency switching, the continuous accumulation and release of magnetic energy guarantees an output voltage that exceeds the input.

By applying Kirchhoff's circuit laws to these operating states, the dynamic continuous-time behavior of the Boost converter over one switching period can be mathematically represented by the following system of equations:

$$\begin{cases} C_1 \frac{dv_{in}(t)}{dt} = i_{in}(t) - i_L(t) \\ C_2 \frac{dv_{out}(t)}{dt} = (1-d) i_L(t) - i_{out}(t) \\ L \frac{di_l(t)}{dt} = v_{in}(t) - (1-d) v_{out}(t) - R_i i_L(t) \end{cases} \tag{2.17}$$

Where $i_{in}(t)$, $i_{iout}(t)$ and $i_L(t)$ are the input, the output and the inductor current, respectively. $V_{in}(t)$, $V_{out}(t)$ and $V_L(t)$ are the input, the output and the inductor voltage.

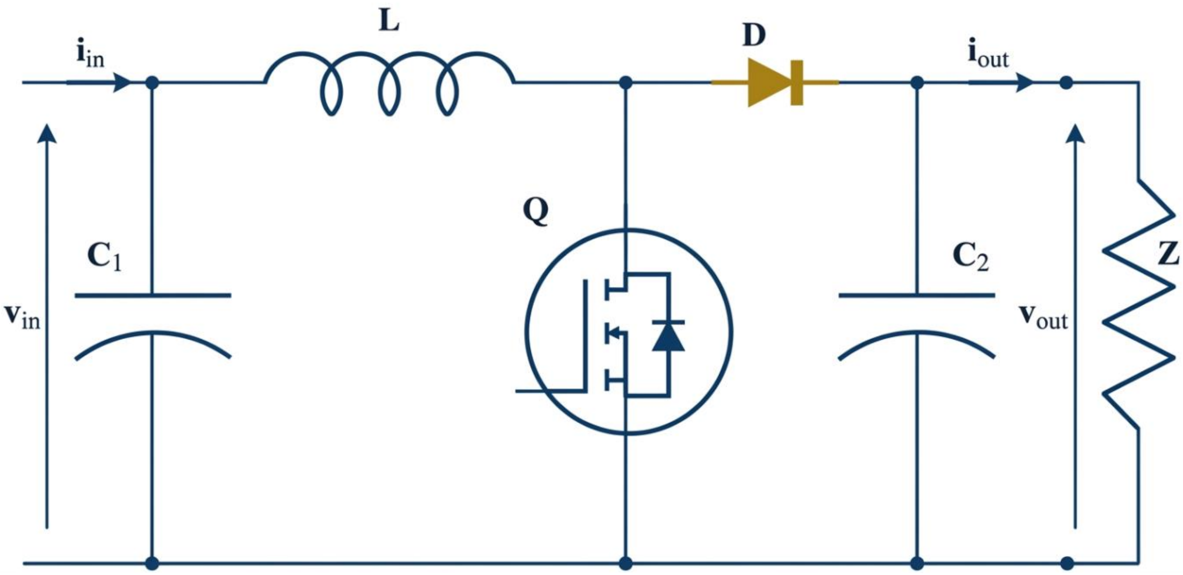


***Figure 2.8: Electrical circuit of a boost converter.***

**2.5. Modeling of the Pumping System :**

As a fundamental component of the hydraulic network, a centrifugal pump is a mechanical machine that transfers rotational kinetic energy into fluid flow and pressure using centrifugal force. The primary objective of these pumps is to elevate fluid pressure and drive water across a designated vertical head and piping distance.

Centrifugal pumps are designed for a relatively fixed full load (Total Dynamic Head). The pump's displacement (volumetric flow) varies proportionally with the motor's rotational speed. The required mechanical torque increases rapidly with speed, while the head is a function of the square of the motor speed. Furthermore, the energy consumption, which is proportional to both flow and head, changes proportionally to the cube of the velocity. Centrifugal pumps are typically utilized at medium or shallow depths (10 to 100 meters) to provide high flow rates.

The fundamental operation of the centrifugal pump is characterized by three interrelated parameters: head ($H$), volumetric flow rate ($Q$), and power ($P$).

$$f(H, Q, P) = 0 \tag{2.18}$$

During pump operation, the system experiences inherent pressure losses, classified primarily as linear (frictional) pressure drops along the pipes and singular (local) pressure drops at fittings. These are mathematically represented by the following relationships:

$$\Delta H_1 = \lambda \frac{V^2}{2\,.g} \cdot \frac{L}{D} \tag{2.19}$$

$$\Delta H_2 = \varepsilon \frac{V^2}{2\,.g} = \varepsilon \frac{8Q^2}{\pi^2 D^2 g} \tag{2.20}$$

With:

- λ :Coefficient of linear pressure drop
- $D$:Internal diameter of the pipe [m]
- $V$: Average velocity of the fluid [m/s]
- $g$: Acceleration of gravity [m/s²]
- $L$: Length of the pipe [m]
- $\mathcal{E}$: Coefficient of local (singular) pressure drop
- $Q$: Volume flow [m³/s]

Furthermore, the functional relationship between the pump's instantaneous rotational speed $N(t)$and its resulting hydraulic performance is governed by the affinity laws. Based on the nominal maximum characteristics of the pump, the instantaneous total head $H(t)$, volumetric flow $Q(t)$, and hydraulic power $H(p)$are given by the following relations:

$$H(t) = H_m.\left(\frac{N(t)}{N_m}\right)^2 \tag{2.21}$$

$$Q(t) = Q_m.\left(\frac{N(t)}{N_m}\right) \tag{2.22}$$

$$H_p = \rho * g * Q * H \tag{2.23}$$

Where:

- H: Total head achieved by the pump [m]
- Hm: Maximum head [m]
- N(t): Instantaneous speed [rpm]
- Nm: Maximum speed [rpm]
- Q(t): Instantaneous flow rate [m3/s]
- Qm: Maximum flow rate [m3/s]
- ρ: Density of the liquid [kg/m3]
- g: Acceleration of gravity [$m/s^2$].

The specific centrifugal pump parameters and general physical constants utilized in this system modeling are defined in Table 2.2.

| Parameter Name | Symbol | Value | Unit |
|---|---|---|---|
| **Synchronous Reluctance Motor (SynRM) Parameters** | | | |
| Stator Phase Resistance | $R_s$ | 2.875 | Ω |
| d-axis Inductance | $L_d$ | 8.5 x $10^{-3}$ | H |
| q-axis Inductance | $L_q$ | 8.5 x $10^{-3}$ | H |
| Moment of Inertia | $J$ | 0.8 x $10^{-3}$ | Kg.$m^2$ |
| Viscous Friction Coefficient | $F$ | 1 x $10^{-3}$ | |
| Number of Pole Pairs | $P$ | 4 | - |
| **Centrifugal Water Pump Parameters** | | | |
| Nominal Speed | $\omega_{nom}$ | 3000 | rpm |
| Nominal Mechanical Power | $P_{nom}$ | 1500 | W |
| Nominal Flow Rate | $Q_{nom}$ | 0.0033 | $m^3/s$ |
| Water Density | $\rho$ | 1000 | Kg/$m^3$ |
| Gravity Acceleration | $g$ | 9.81 | m/$s^2$ |

***Table 2.2: Centrifugal pump and Synch motor parameters***

**2.6. Conclusion :**

In this chapter, the comprehensive study and mathematical modeling of a Photovoltaic Water Pumping System were presented. The chapter established the dynamic models for the PV array, the Boost DC-DC converter, and the Synchronous Reluctance Motor (SynRM) driven by a three-phase voltage source inverter. Crucially, the system is designed to be controlled via Finite Control Set Model Predictive Control (FCS-MPC), an advanced technique that directly evaluates the discrete states of the inverter to optimize SynRM operation, completely eliminating the need for traditional carrier-based PWM modulators. Finally, the mechanical load was accurately represented by establishing the governing hydraulic equations of the centrifugal water pump.

# Chapter 3

# Simulation Results of the FCS-MPC and MPPT Strategies

### 3.1. Introduction :

While the fundamental physics and mathematical models of the Photovoltaic Water Pumping System (PVWPS) were established in the previous chapter, the overall efficiency of the energy conversion chain relies entirely on the robustness of its control architecture. Maximizing operational efficiency is paramount to ensure the technical reliability and economic viability of the standalone system.

As demonstrated in the established power-voltage (P-V) characteristics, a PV array possesses a unique Maximum Power Point (MPP) where the module produces its peak power output $P_{max}$. However, this optimal coordinate is highly nonlinear and constantly shifts depending on instantaneous meteorological conditions. To ensure the system operates precisely at this optimal point, an intermediate control stage is required. Furthermore, the extracted DC power must be optimally inverted to drive the Synchronous Reluctance Motor (SynRM) and its coupled centrifugal pump.

Consequently, this chapter details the design and simulation of the two primary control systems: the Maximum Power Point Tracking (MPPT) algorithm governing the DC-DC Boost converter, and the Finite Control Set Model Predictive Control (FCS-MPC) strategy governing the three-phase voltage source inverter.

### 3.2. Maximum Power Point Tracking (MPPT) :

As previously established, the power generated by a photovoltaic array is heavily dictated by fluctuations in solar irradiance and ambient temperature. Because the electrical characteristics of a PV module are highly nonlinear, there exists only one unique operating coordinate on the P-V curve, the Maximum Power Point (MPP), where the array delivers its absolute maximum possible power ($P_{max}$).

To mitigate environmental disturbances and continuously extract this peak power, a Maximum Power Point Tracking (MPPT) control system is strictly required. The MPPT controller acts as the core decision-making unit, continuously monitoring the PV array's instantaneous voltage and current to dynamically locate and maintain operation at the MPP, regardless of shifting meteorological conditions or changing mechanical load demands from the pumping system.

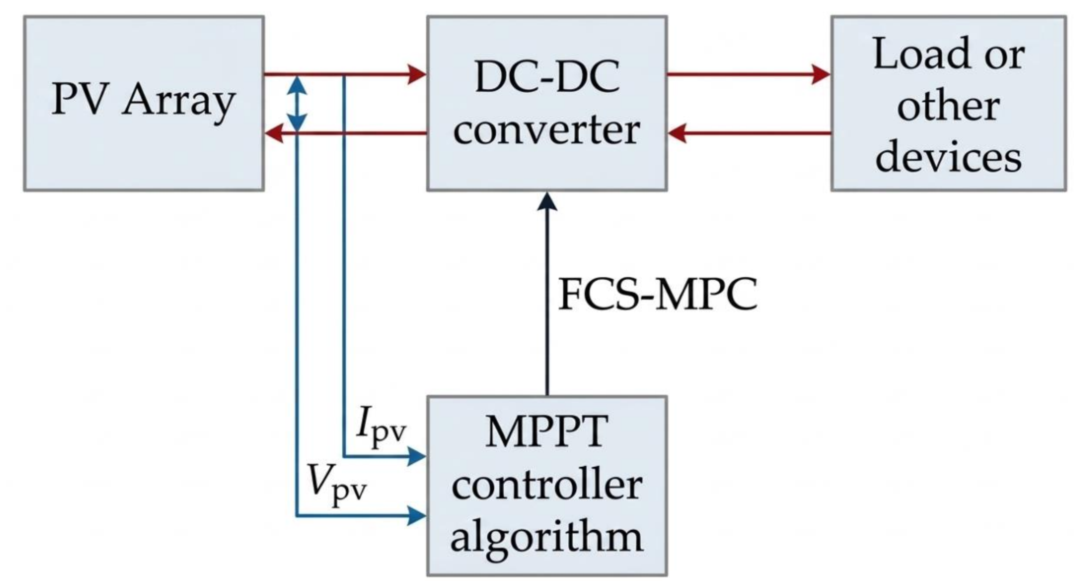


***Figure 3.1: MPPT system diagram***

### 3.2.1. DC to DC Converter :

In order to transmit maximum power from the source to the load, the MPPT system essentially acts as an active impedance matcher. By utilizing algorithms to dictate the switching state of the DC-DC converter, the controller continuously aligns the apparent impedance of the system load with the internal impedance of the PV source [16].

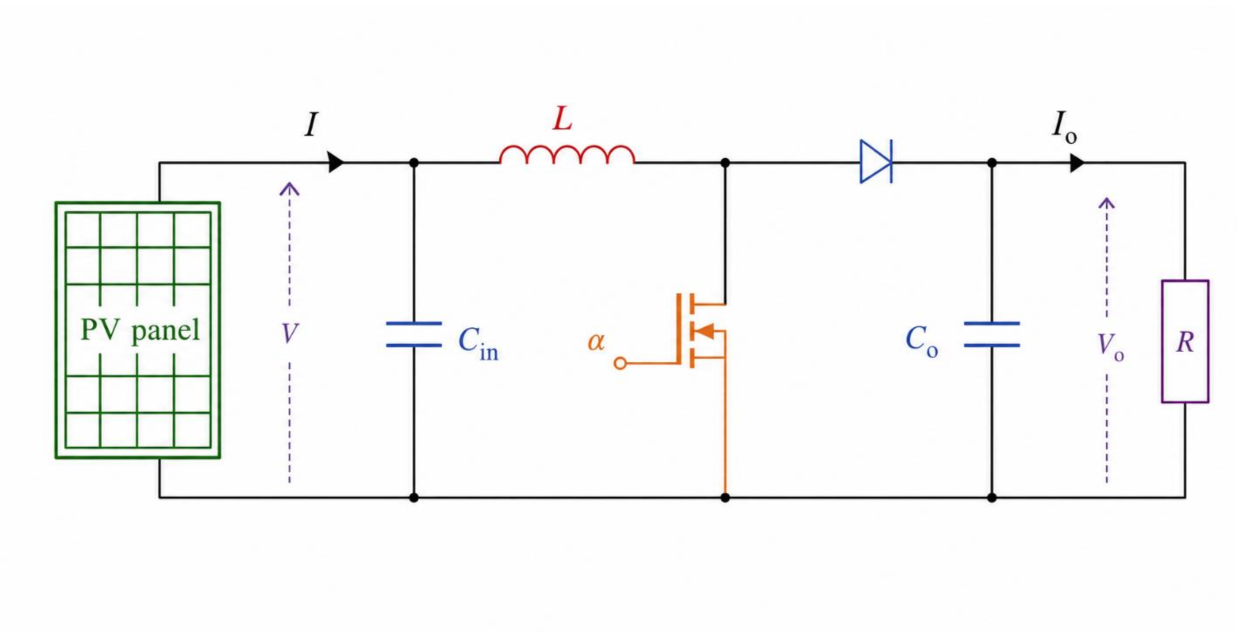


***Figure 3.2: Boost Converter in an MPPT based PV System***

**The operation principle of this converter is described by the following equations:**

$$V_0 = \frac{V}{1-D} \tag{3.1}$$

$$I_0 = I(1-D) \tag{3.2}$$

Based on the aforementioned mathematical relationships, the equivalent input resistance perceived at the PV array terminals $R_{eq}$can be expressed as a function of the actual load resistance $R$ as follows :

$$R_{eq} = \frac{V}{I} = \frac{V_0(1-D)^2}{I_0} = R(1-D)^2 \tag{3.3}$$

Consequently, the optimal switching duty cycle $d$ required by the MPPT controller to synthesize this equivalent resistance and extract maximum power is calculated using the following expression:

$$D = 1 - \sqrt{\frac{R_{eq}}{R}} \quad (3.4)$$

Where $d$ denotes the optimal switching duty cycle, and $R$represents the specific system resistance at which peak power extraction is achieved.

$$R = \frac{V_{Mpp}}{I_{Mpp}} \quad (3.5)$$

### 3.2.2. Classification of MPPT Strategies :

Maximum Power Point Tracking algorithms can be broadly categorized based on their hardware implementation (analog, digital, or mixed-signal). However, from a control theory perspective, it is far more rigorous to classify them according to their tracking methodology and required input variables. These algorithms generally fall into two primary classifications:

**A. Indirect MPPT Techniques:**

Indirect methods estimate the approximate location of the MPP utilizing prior knowledge of the PV panel's physical characteristics or through established empirical relationships. These techniques typically rely on measuring quasi-static parameters, such as a fraction of the open-circuit voltage $V_{oc}$ or short-circuit current$I_{sc}$, to approximate the optimal operating point. While computationally simple, they lack the ability to dynamically adapt to unexpected operational variations, degradation over time, or partial shading conditions.

**B. Direct MPPT Techniques:**

In contrast, direct methods continuously measure the instantaneous dynamic variables of the system ,specifically the PV array voltage and currentto calculate the real-time output power. By actively evaluating the mathematical gradient of the P-V curve, direct algorithms can dynamically locate and track the true MPP even under rapidly fluctuating environmental conditions. The Perturb and Observe (P&O) algorithm utilized in this system is a fundamental example of a highly effective direct tracking technique.

### 3.2.3. Perturb and Observe (P&O) Algorithm :

Among the various MPPT techniques documented in the literature, the Perturb and Observe (P&O) algorithm is the most widely implemented due to its structural simplicity, ease of integration, and relatively low computational demand.

The fundamental operational principle of the P&O algorithm relies on intentionally introducing a deliberate, periodic perturbation, specifically, a small incremental change to the operating voltage of the PV array (or directly to the duty cycle of the Boost converter). By continuously measuring the instantaneous photovoltaic voltage $V_{pv}$ and current $I_{pv}$ , the controller calculates the instantaneous output power $P_{pv}(k)$. This current power value is then compared to the power calculated during the previous sampling period ($P_{pv}(k-1)$) to determine the differential change in power ($\Delta P$).

The algorithm evaluates the system based on the following logical conditions:

- If the perturbation results in an increase in power ($\Delta P > 0$), it indicates that the operating point is moving toward the Maximum Power Point (MPP). Consequently, the controller applies the next perturbation in the **same direction**.
- Conversely, if the perturbation results in a decrease in power ($\Delta P < 0$), it indicates that the operating point has moved away from the MPP. The controller immediately reverses the sign of the perturbation, moving the operating point in the **opposite direction**.

This continuous process of "perturbing and observing" forces the system to climb the P-V

characteristic curve until it reaches the peak. Once at the MPP, the operating point will inherently oscillate slightly around the maximum value. The magnitude of this steady-state oscillation is directly proportional to the chosen perturbation step size.

The logical sequence and decision-making architecture of the implemented P&O algorithm are visually summarized in the flowchart presented in Figure 3.3.

The algorithm outputs an optimal

reference signal, which is subsequently translated into the switching duty cycle ($d$) applied to the active gate of the DC-DC Boost converter[21][22]

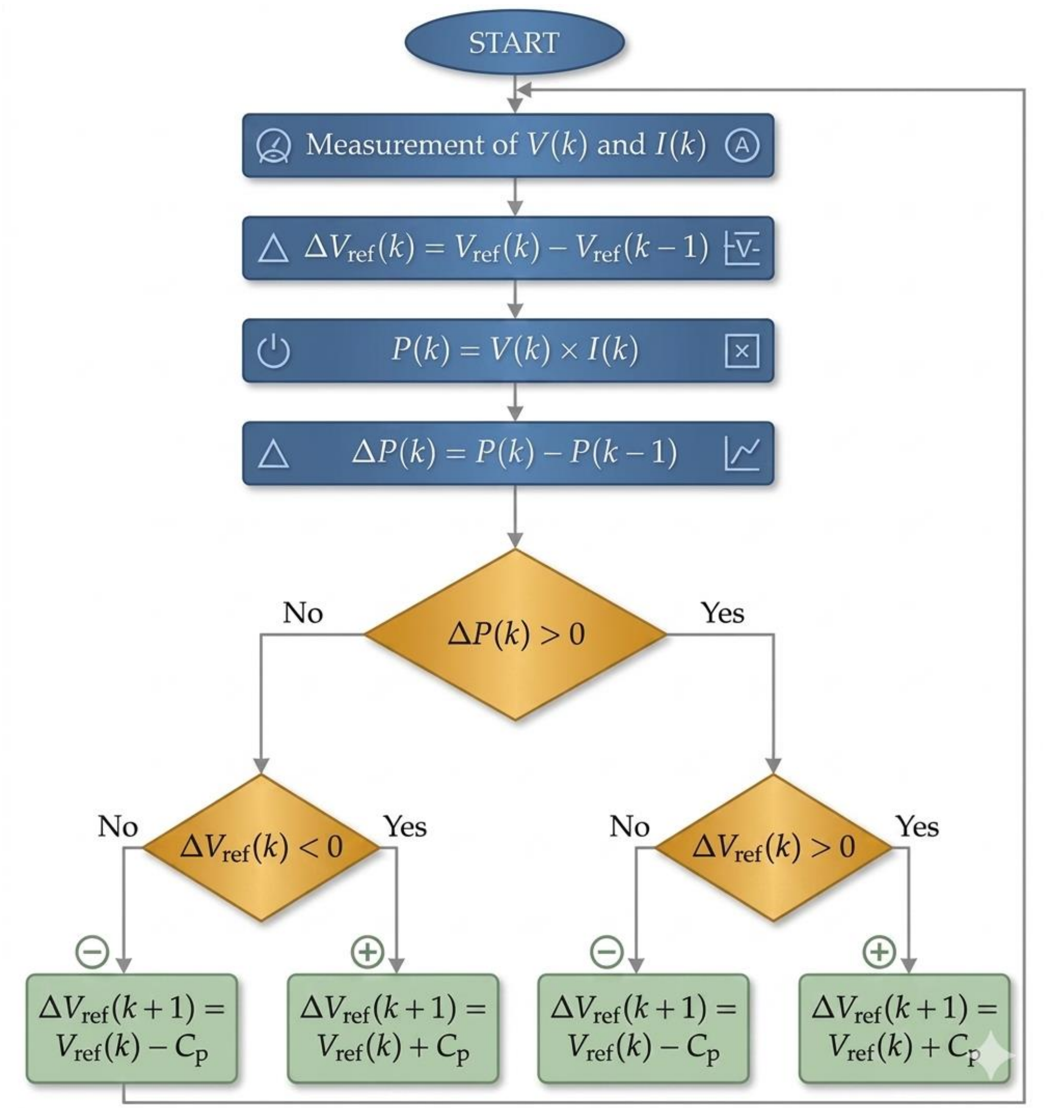


***Figure 3.3: Flowchart of the Perturb & Observe MPPT algorithm.***

### 3.3. Finite Control Set Model Predictive Control (FCS-MPC) of SynRM :

Traditionally, the control of Synchronous Reluctance Motors (SynRM) has been dominated by linear control strategies, most notably Field Oriented Control (FOC). While FOC is well-established, it inherently relies on cascaded Proportional-Integral (PI) controllers and requires a continuous modulation stagesuch as Pulse Width Modulation (PWM)to generate the required switching states. This approach limits the dynamic transient response of the system and complicates the tuning process.

In contrast, Finite Control Set Model Predictive Control (FCS-MPC) represents a fundamental paradigm shift in modern power electronics control. FCS-MPC completely eliminates the inner current PI controllers and the PWM modulator. Instead, it leverages the inherently discrete nature of the three-phase Voltage Source Inverter (VSI). By utilizing the mathematical model of the SynRM, the controller predicts the future behavior of the machine's currents for every possible switching state of the inverter. A predefined mathematical cost function is then evaluated for each prediction, and the optimal switching state is selected and applied directly to the inverter gates.

#### 3.3.1. Discrete-Time Predictive Model :

To predict the future behavior of the motor, the continuous-time dynamic equations of the SynRM must be discretized. Using the forward Euler approximation method with a discrete sampling time of $T_s$, the continuous derivatives of the direct and quadrature axis currents are approximated as:

$$\frac{d_{id}}{dt} \approx \frac{i_d(k+1) - i_d(k)}{T_s} \tag{3.6}$$

$$\frac{d_{iq}}{dt} \approx \frac{i_q(k+1) - i_q(k)}{T_s} \tag{3.7}$$

By substituting these discrete approximations into the continuous state-space model, the predicted future currents at the next instant $(k + 1)$ can be algebraically isolated.

The discrete-time predictive model of the SynRM is therefore expressed as:

$$i_d(k+1) = i_d(k) + \frac{T_S}{L_d}(V_d(k) - R_s i_d(k) + \omega_e L_q i_q(k)) \quad (3.8)$$

$$i_q(k+1) = i_q(k) + \frac{T_S}{L_q}(V_q(k) - R_s i_q(k) - \omega_e L_d i_d(k)) \quad (3.9)$$

Where $i_d(k)$ and $i_q(k)$ are the measured stator currents at the current sampling instant, $\omega_e$is the electrical rotor speed, and $V_d(k)$ and $V_q(k)$ represent the $d-q$axis voltages applied by the inverter.

**3.3.2. Cost Function Optimization and Reference Generation :**

A standard two-level, three-phase VSI possesses $2^3 = 8$ possible switching states, comprising six active voltage vectors and two zero voltage vectors. For every single control cycle, the microprocessor transforms these 8 voltage vectors into the synchronous $d-q$ reference frame and feeds them into the predictive equations above, generating 8 distinct predictions for the future currents: $i_d^p$and $i_q^p$.

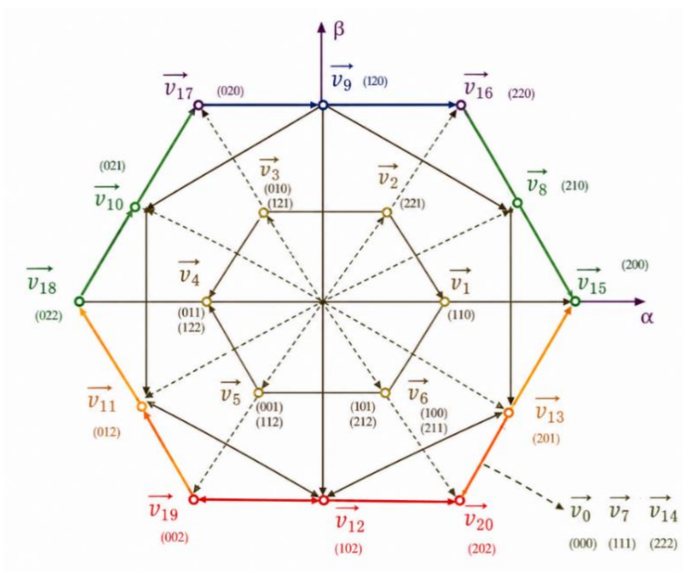

*Figure 3.4: The eight active and zero voltage vectors generated by a two-level three-phase voltage source inverter*

To determine the optimal switching state, a cost function $g$ is evaluated for each of the 8 predictions. The primary objective of the FCS-MPC in this system is absolute current tracking accuracy. Therefore, the cost function is defined as the absolute squared error between the reference currents ($i_d^*$ and $i_q^*$) and the predicted currents:

$$g = (i_d^* - i_d^p)^2 + (i_q^* - i_q^p)^2 \tag{3.10}$$

The control algorithm evaluates this function for all 8 available voltage vectors. The specific switching state that yields the minimum value for $g$ is locked in and directly fired to the insulated-gate bipolar transistors (IGBTs) of the inverter for the upcoming $(k + 1)$ interval.

While the highly dynamic inner current control loop is governed by this discrete FCS-MPC algorithm, the outer speed regulation loop utilizes a standard Proportional-Integral (PI) controller. The measured mechanical speed of the SynRM rotor ($\Omega_m$) is compared to the reference speed ($\Omega_m^*$) dictated by the MPPT-driven pump requirements. The resulting speed error is processed by the PI controller to generate the reference electromagnetic torque ($T_e^*$) required to maintain the desired flow rate.

To minimize stator copper losses and maximize the overall energy efficiency of the drive system, the Maximum Torque Per Ampere (MTPA) control strategy is implemented. Because the SynRM lacks a permanent magnet excitation source or rotor windings, electromagnetic torque is generated entirely by the magnetic reluctance variance between the direct and quadrature axes. The MTPA algorithm mathematically determines the optimal current vector trajectory. For any given reference torque ($T_e^*$), the MTPA block calculates the precise combination of direct-axis ($i_d^*$) and quadrature-axis ($i_q^*$) currents that will synthesize that torque using the absolute minimum total stator current magnitude.

These optimally calculated reference currents, $i_d^*$ and $i_q^*$, are subsequently fed directly into the FCS-MPC cost function ($g$) as the target tracking variables, seamlessly unifying the efficiency optimization of the MTPA with the extreme dynamic performance of the predictive controller.

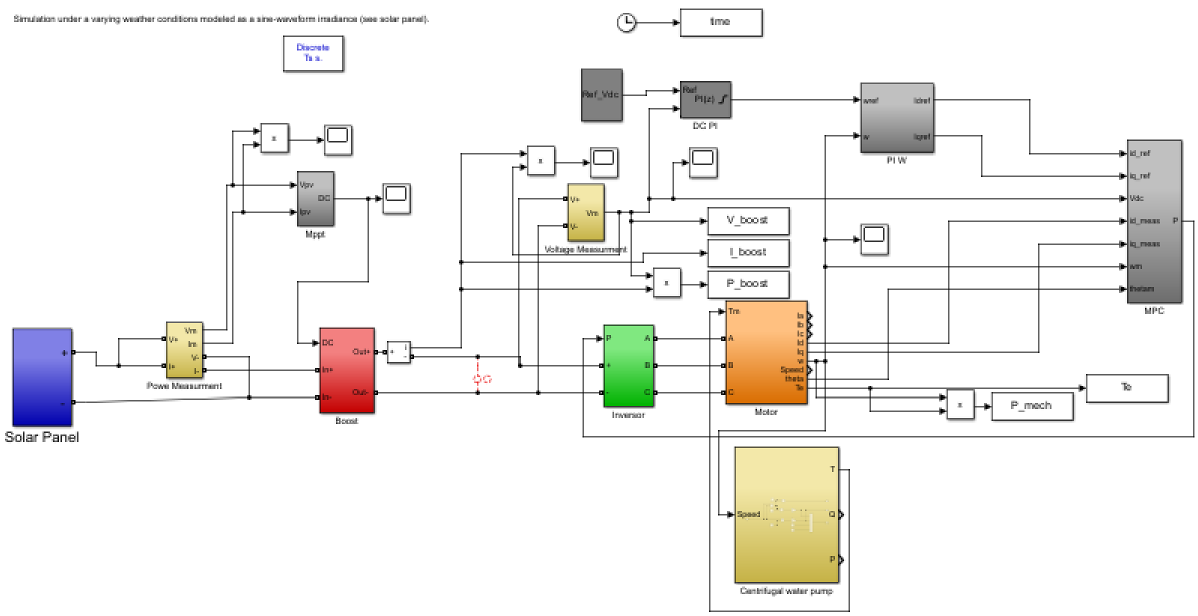


***Figure 3.5: Complete global block diagram of the proposed FCS-MPC and MTPA control strategy for the SynRM***

## 3.4.Simulation Results and Discussion :

### 3.4.1.Test Scenario Definition:

The system was evaluated against a highly dynamic 20-second solar irradiance profile to test its resilience to abrupt atmospheric changes, moving beyond standard static testing. With the module temperature fixed at 25°C, the programmed profile includes:

- **0s to 4s (Startup):** Step-wise irradiance increments (500, 800, and 1000 W/m²) to test the system's initialization sequence and MPPT tracking speed.

- **8s to 12s (Heavy Cloud Cover):** A sharp decline to 200 W/m² to evaluate the DC link regulation and confirm the motor continues to operate under severe energy constraints.
- **12s to 20s (Dynamic Recovery):** A rapid return to 1000 W/m², followed by a drop to 700 W/m² at t=16s, designed to prove the controller maintains stable, error-free tracking during rapidly shifting weather patterns.

### 3.4.2. Irradiance And Photovoltaic Array Performance :

The first stage of the system evaluation establishes the environmental conditions applied to the photovoltaic array. To rigorously test the robustness of the system, a dynamic multi-step solar irradiance profile was programmed, as detailed in **Table 3.1** and illustrated in **Figure 3.6**

| **Time (S)** | $0-1$ | $1-4$ | $4-8$ | $8-12$ | $12-16$ | $16-20$ |
|---|---|---|---|---|---|---|
| **Irradiance(W/$m^2$)** | 500 | 800 | 1000 | 200 | 1000 | 700 |

***Table 3.1: Irradiance change per time***

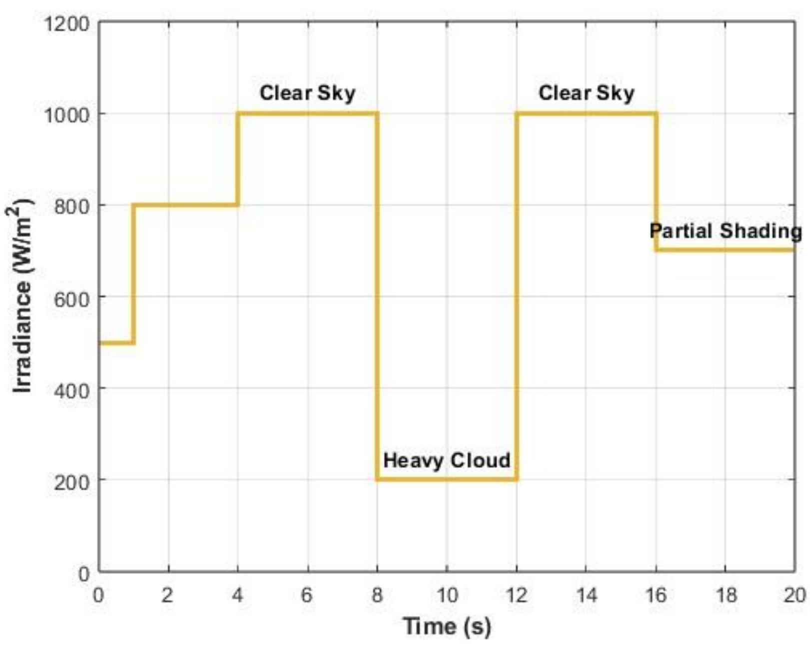


***Figure 3.6 :Evolution of solar irradiance over time***

The subsequent figures illustrate the dynamic electrical response of the PV array as it reacts to these varying atmospheric conditions.

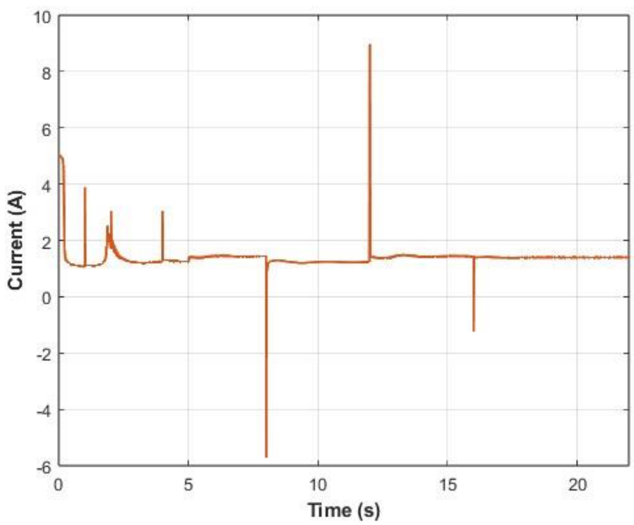


***Figure 3.7 :PV Array Current$I_{pv}$***

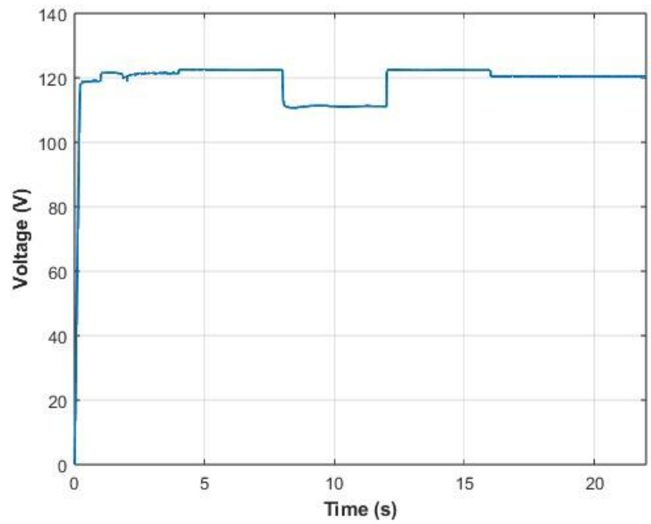


***Figure 3.8: PV Array Voltage$V_{pv}$***

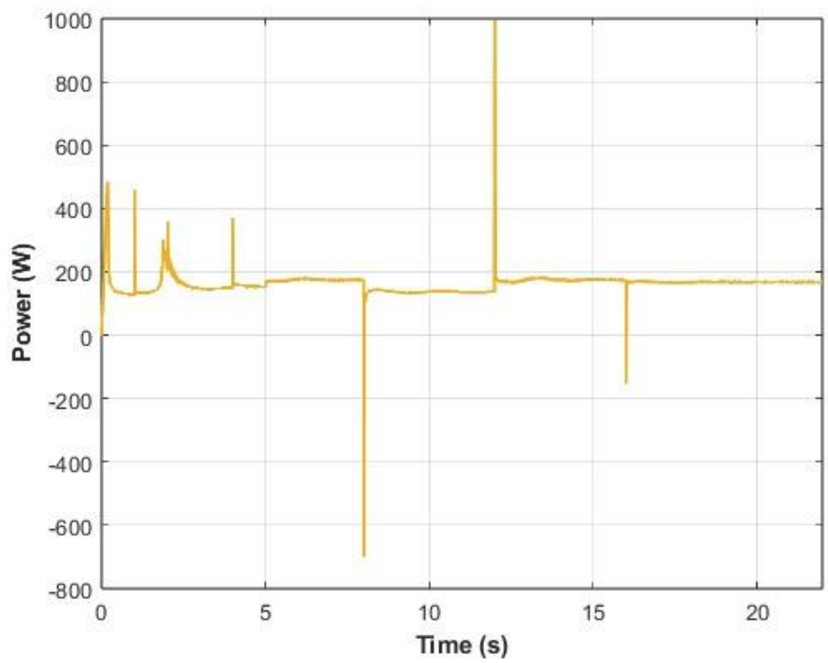


***Figure 3.9 :PV Array Output Power$P_{pv}$***

The figures demonstrate the behavior of the photovoltaic array over the 20-second simulation profile, designed to emulate real-world meteorological events:

**0s to 8s (Startup and Clear-Sky Conditions):**

During the initial 4 seconds, the system is subjected to sequential irradiance steps (500, 800, and 1000 W/m²). This physical profile simulates the gradual clearing of morning atmospheric cover, designed to test the initial tracking speed of the MPPT. At t = 5 s, the algorithm activates, bringing the PV voltage to its Maximum Power Point (MPP) near 120 V. The system successfully extracts the nominal 1000 W and maintains perfect stability, demonstrating optimal steady-state operation under ideal clear-sky conditions.

**8s to 12s (Heavy Cloud Cover / Severe Shading):**

At t = 8 s, the irradiance is abruptly reduced to 200 W/m². This physical change represents a dense cloud passing directly over the PV array, casting a heavy shadow. Consequently, the available solar energy is severely restricted; the PV current decreases to approximately 1.5 A, and the output power falls to 200 W. The purpose of this extreme scenario is to verify the

system's resilience against DC bus collapse. Despite the energy deficit, the MPPT controller successfully adjusts the duty cycle to maintain the PV voltage near 110 V, ensuring the system remains operational rather than stalling.

**12s to 20s (Cloud Clearance and Partial Shading):**

At t = 12 s, the irradiance returns to 1000 W/m², simulating the dense cloud passing completely and exposing the array to full, direct sunlight. The control system demonstrates robust transient recovery, returning to peak power generation without triggering dangerous electrical overshoots. Finally, at t = 16 s, the irradiance is reduced to 700 W/m² to emulate a partial shading event caused by light, semi-transparent cloud cover. The controller accurately tracks this moderate change, proving continuous, proportional power extraction without steady-state error under shifting weather.

### 3.4.3. Boost Converter and DC Link Dynamics:

The second stage of the system evaluation focuses on the intermediate power processing and voltage regulation. The following figures illustrate the dynamic electrical response of the DC-DC Boost Converter and the DC link as the system reacts to the programmed weather profile.

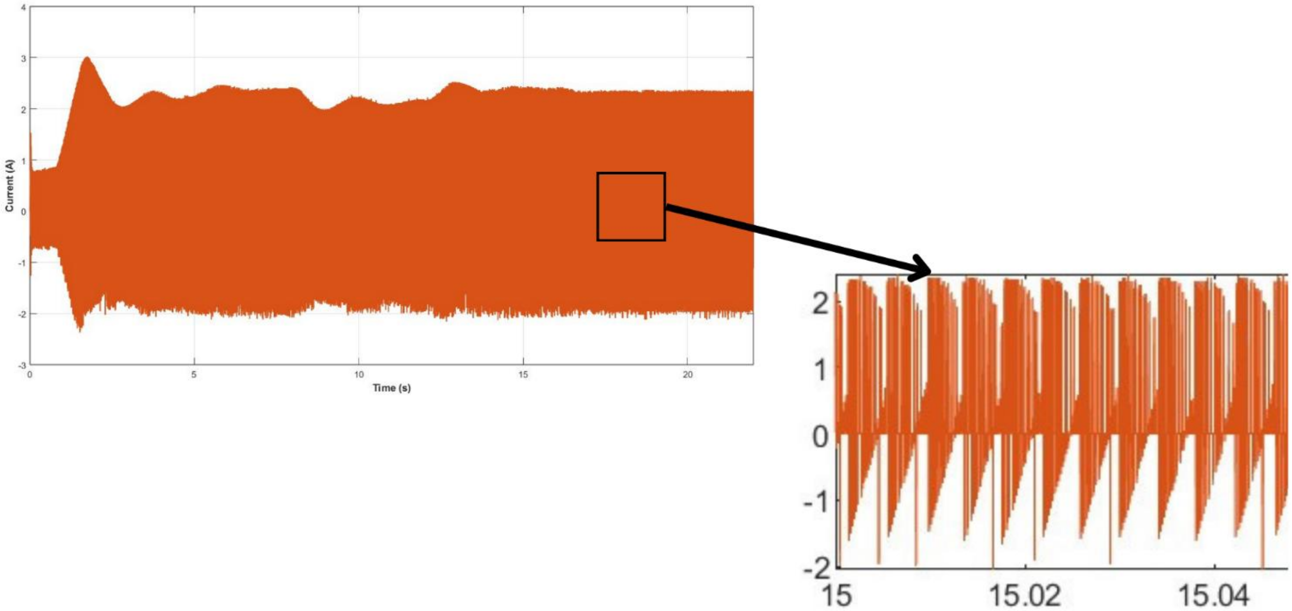


***Figure 3.10 :Output Current with steady-state switching detail*** $(I_b)$

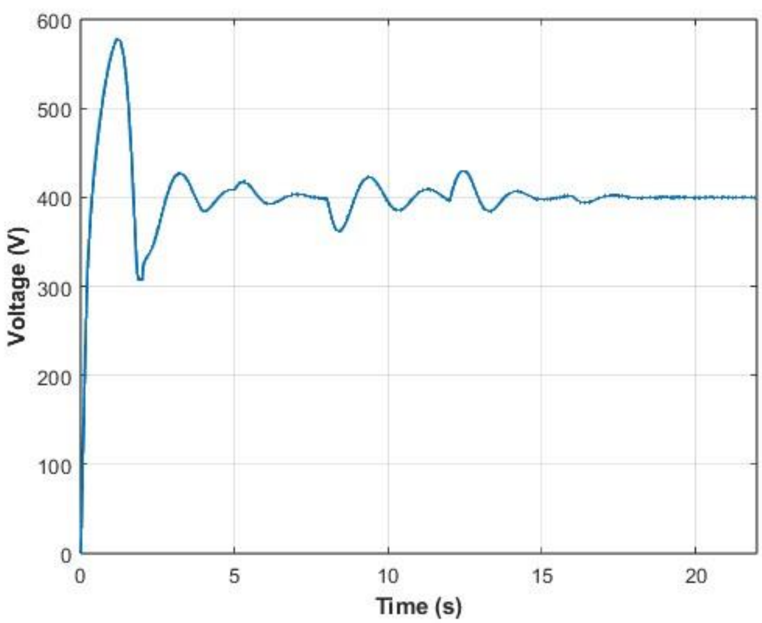


***Figure 3.11 :DC Link Voltage***$(V_b)$

The Boost Converter serves as the critical intermediate power processing stage. Its primary function is to elevate the varying PV array voltage while maintaining a rigid, stable DC link for the downstream motor inverter. Its performance across the 20-second meteorological profile is analyzed below:

**0s to 8s (Startup and Clear-Sky Conditions):**

During the first 4 seconds, the irradiance sequentially increases (500, 800, and 1000 $W/m^2$), physically simulating the gradual dissipation of morning cloud cover. The boost converter successfully steps up this varying input to meet the required DC link reference. As the MPPT algorithm converges at t = 5 s, the transmitted power stabilizes at approximately 1000 W. Crucially, the DC bus voltage settles smoothly at the 400 V reference dictated by the outer-loop PI speed controller. This establishes a stiff, reliable DC source for the motor prior to any atmospheric disturbances.

**8s to 12s (Heavy Cloud Cover and Severe Shading):**

At t = 8s, a dense cloud blocks the solar array, physically restricting the available irradiance to 200 $W/m^2$. Consequently, the power transmitted through the boost converter drops drastically to approximately 200 W, accompanied by a proportional fall in output current. However, the DC link voltage exhibits remarkable resilience. Rather than collapsing under this severe energy deficit, the voltage remains strictly regulated near 400 V. This confirms that the PI controller successfully decoupled the mechanical load, actively reducing the motor's power demand to match the restricted solar supply, thereby preserving the electrical integrity of the entire system.

**12s to 20s (Cloud Clearance and Steady-State Ripple):**

At t = 12 s, the dense cloud passes entirely, restoring full irradiance (1000 $W/m^2$). The converter immediately processes the peak power, and the resulting transient voltage spike on the DC link is rapidly damped by the PI controller. To explicitly illustrate the high-frequency switching dynamics during this clear-sky steady-state operation, inset plots are provided at t = 15 s for both current and power. These detailed views reveal the characteristic continuous conduction mode (CCM) switching ripple. The ripple amplitude is tightly bounded, verifying the correct sizing of the passive components (inductor and capacitor).

Finally, a light, semi-transparent cloud reduces irradiance to 700 $W/m^2$ at t = 16 s; the converter smoothly tracks this moderate drop, ensuring uninterrupted power delivery to the FCS-MPC stage without steady-state error.

### 3.4.4. Predictive Controller Tracking and Mechanical Output :

Before observing the final electromechanical rotation, it is crucial to validate the internal tracking accuracy of the Finite Control Set Model Predictive Controller (FCS-MPC). For the synchronous motor, the control strategy is executed in the rotating $d - q$ reference frame. The following figures illustrate the algorithm's ability to track the optimal dynamic current references and generate the necessary mechanical torque.

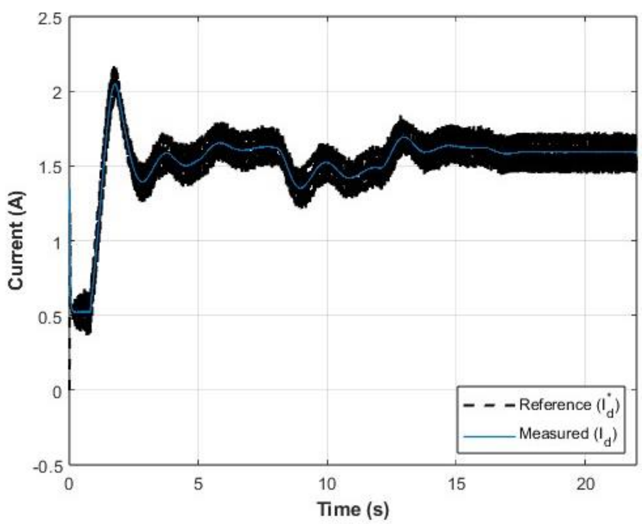


*Figure 3.12:d-axis Current Tracking ($I_d$)*

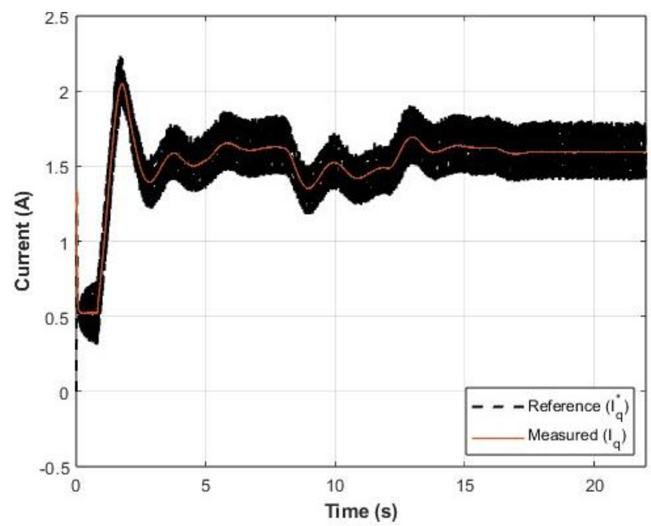


*Figure 3.13:q-axis Current Tracking ($I_q$)*

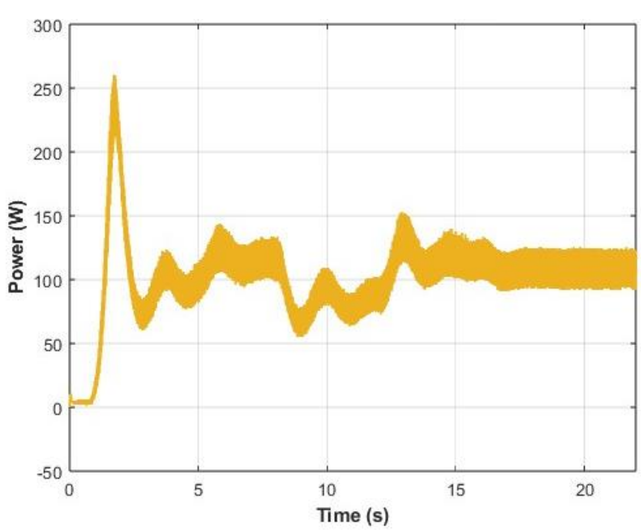


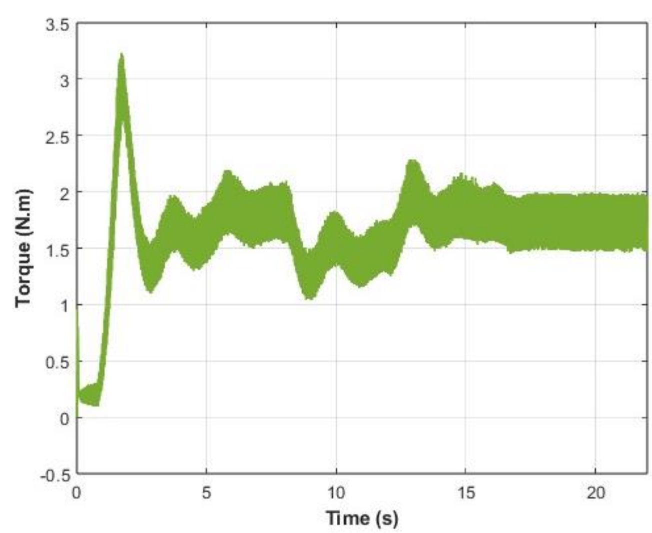


*Figure 3.14: Mechanical Power ($P_{mech}$)Figure 3.15: Electromagnetic Torque ($T_e$)*

The FCS-MPC continuously evaluates a discrete cost function to minimize the error between the measured $d - q$ currents and their reference values. The tracking performance across the dynamic weather profile is analyzed as follows:

**0s to 8s (Startup and Clear-Sky Conditions):**

As the morning irradiance physically increases, the outer PI speed loop dictates the required torque-producing current ($I_q^*$) Simultaneously, rather than forcing the flux-producing current to zero, the control architecture actively calculates a dynamic, non-zero $d$-axis reference ($I_d^*$). This advanced tracking ensures optimal magnetic flux and Maximum Torque Per Ampere (MTPA) operation. As shown in Figures W-a and W-b, the FCS-MPC tracks both $I_d^*$ and $I_q^*$ with exceptional accuracy and minimal ripple. Consequently, the electromagnetic torque ($T_e$) rises proportionally, and the generated mechanical power ($P_{mech}$) stabilizes near 120 W under clear-sky conditions at t = 5 s.

**8s to 12s (Heavy Cloud Cover and Severe Shading):**

At $t = 8\,s$, the dense cloud simulation severely restricts available solar energy. To prevent the DC bus voltage from collapsing, the controller instantly reduces the speed command, directly lowering the $I_q$ demand. The actual $I_q$ current accurately follows this sharp drop, resulting in an immediate reduction in electromagnetic torque and mechanical power (dropping to approximately 60 W). Notably, the dynamic $I_d$ reference adjusts proportionally, and the measured $I_d$ tracks this reduction perfectly, ensuring the motor maintains optimal efficiency even during severe energy deficits.

**12s to 20s (Cloud Clearance and Dynamic Load):**

Following the passing of the dense cloud at $t = 12$ s, the current references spike to rapidly re-accelerate the motor. The FCS-MPC tracking instantly matches this demand, generating the high torque peak required for mechanical recovery. During the final partial shading event at $t = 16$ s, the controller ensures both the $d - axis$ and $q - axis$ currents, along with the resulting mechanical power, smoothly step down without steady-state error. This pristine internal tracking proves that the controller can deliver highly reliable, optimized mechanical power to the downstream hydraulic pump under all atmospheric variations.

### 3.4.5. Motor Speed and Stator Current Dynamics:

The next stage of the system evaluation focuses on the electromechanical performance of the motor-pump assembly. The following figures illustrate the dynamic mechanical speed and stator current response of the Synchronous Reluctance Motor (SynRM) as it is driven by the predictive controller (FCS-MPC) throughout the programmed weather profile.

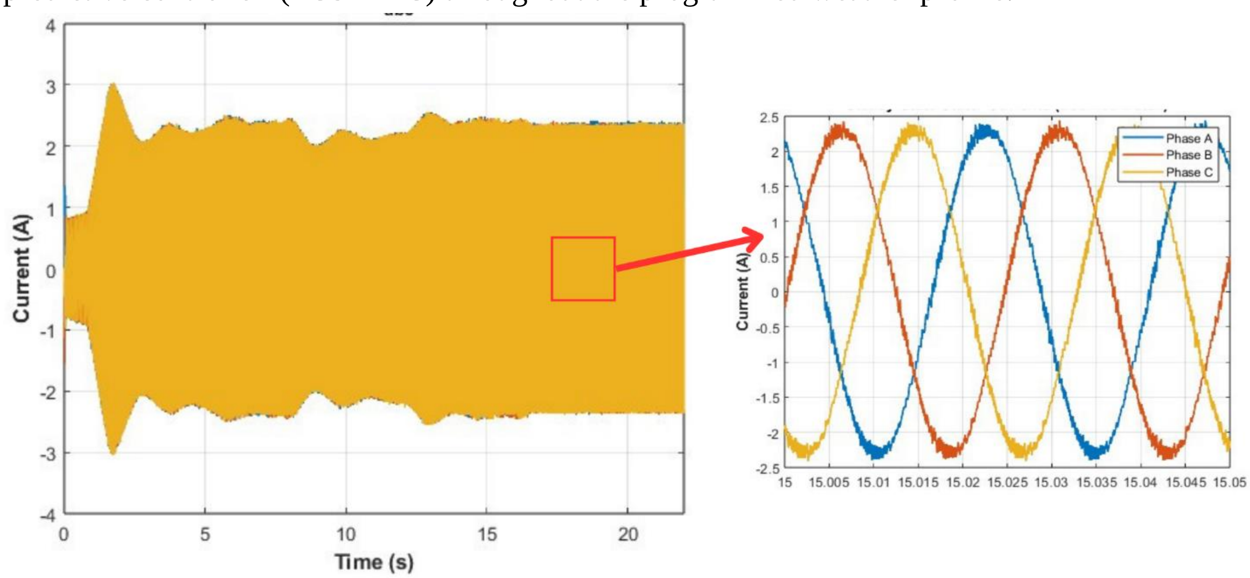


***Figure 3.16:Three-Phase Stator Currents ($I_{abc}$) with steady-state waveform detail under FCS-MPC control***

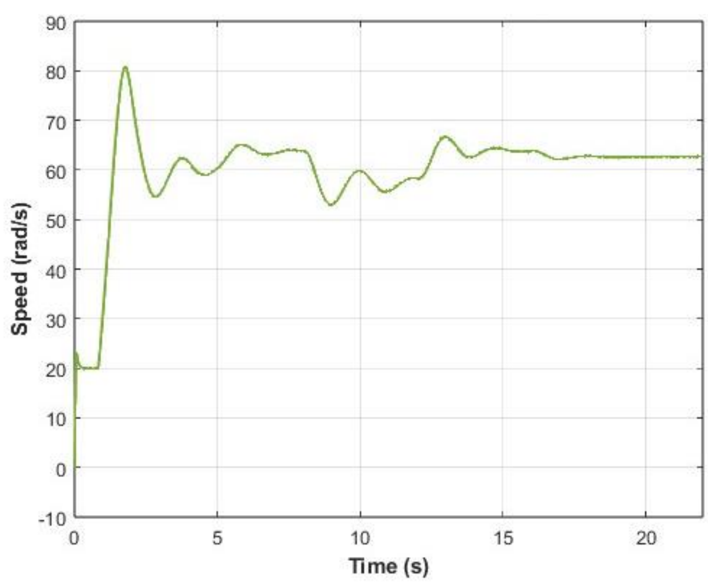


***Figure 3.17 :Dynamic response of the* SynRM *Motor Rotor Speed ($\omega_m$).***

The final electrical stage of the evaluation observes the electromechanical response of the Synchronous Reluctance Motor (SynRM) driven by the Finite Control Set Model Predictive Controller (FCS-MPC)

**0s to 8s (Startup and Clear-Sky Conditions):**

As the morning irradiance physically increases during the first 4 seconds, the available solar power rises. The outer-loop PI controller commands a progressively higher reference speed, and the motor successfully accelerates, extracting the maximum available power to drive the pump. The FCS-MPC synthesizes the optimal switching states to supply the required three-phase currents smoothly. By t = 5 s, the motor speed stabilizes at its nominal rating, corresponding to the 1000 $W/m^2$ clear-sky condition.

**8s to 12s (Heavy Cloud Cover and Severe Shading):**

When the dense cloud restricts irradiance to 200 $W/m^2$ at $t = 8$ s, the system faces a massive energy deficit. To prevent the DC bus from collapsing, the PI controller actively reduces the motor's speed reference. Consequently, the motor safely decelerates, and the magnitude of the stator currents drops proportionally. The FCS-MPC maintains exceptional control throughout this harsh transient, ensuring the motor continues running at a reduced capacity without losing synchronization or stalling.

**12s to 20s (Cloud Clearance and Steady-State Quality):**

Following the physical cloud clearance at $t = 12\,s$, the motor rapidly and smoothly accelerates back to nominal speed. To demonstrate the power quality delivered by the predictive controller, an inset plot details the stator currents at $t = 15\,s$. The zoomed waveforms exhibit highly sinusoidal profiles with minimal total harmonic distortion (THD), proving the FCS-MPC correctly minimizes the cost function.

Finally, the moderate irradiance drop to 700 $W/m^2$ at $t = 16\,s$ results in a perfectly proportional reduction in mechanical speed, confirming robust, continuous operation under shifting weather constraints.

### 3.4.6. Hydraulic Performance of the Centrifugal Pump :

The ultimate objective of the proposed standalone PV pumping system is the reliable delivery of water under varying atmospheric conditions. To validate this, the mechanical output of the synchronous motor is coupled to a dynamic centrifugal water pump model. The following figures demonstrate the translation of optimized mechanical power into physical hydraulic output

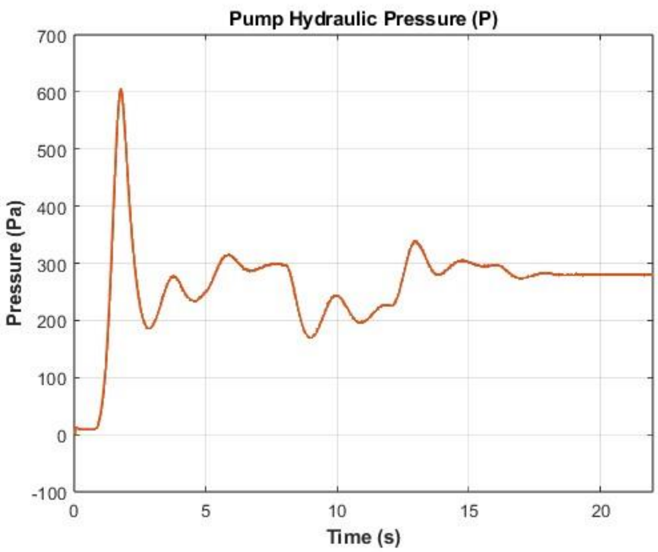


*Figure 3.18 :Hydraulic Pressure (P)*

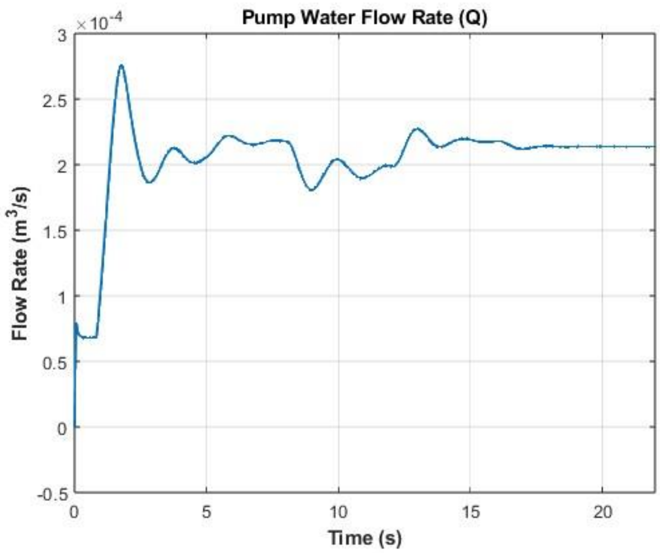


*Figure 3.19 :Water Flow Rate (Q)*

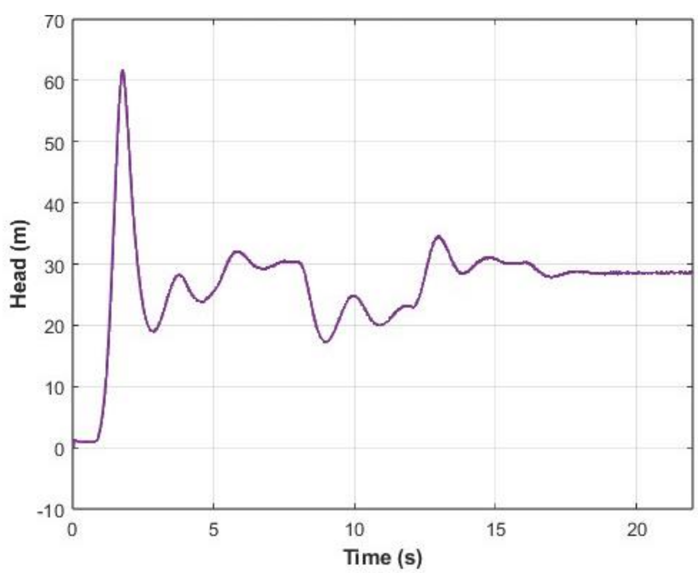


*Figure 3.20 : Total Dynamic Head (H)*

The physical water delivery perfectly reflects the mechanical power regulated by the FCS-MPC throughout the weather profile.

**0s to 8s (Startup and Clear-Sky Conditions):**

During the initial startup phase (0–2 s), the pump must overcome the static inertia of the water resting in the pipe, resulting in a brief, expected transient spike in the dynamic head (reaching approximately 60 m). Following this startup transient, the system quickly stabilizes as the solar irradiance reaches its peak of 1000 $W/m^2$. At t = 5 s, the pump develops a steady-state Total Dynamic Head of approximately 30 meters, driving a continuous water flow rate of $2.2 \times 10^{-4}$ $m^3/s$ (equivalent to roughly 13.2 L/min). This represents the nominal pumping capacity of the system under optimal weather conditions, perfectly suited for standard agricultural borehole depths.

**8s to 12s (Heavy Cloud Cover and Severe Shading):**

When the sudden, dense cloud drops the irradiance to 200 $W/m^2$ at t = 8 s, the available mechanical power decreases. The motor naturally decelerates, reducing the driving force on the pump shaft. Consequently, the dynamic head drops to approximately 20 meters, and the flow rate decreases to roughly $1.9 \times 10^{-4}$ $m^3/s$. Crucially, the flow rate never drops to zero. The predictive controller successfully balances the severe energy deficit, ensuring the pump maintains sufficient pipe pressure to deliver water continuously without stalling.

**12s to 20s (Cloud Clearance and Steady-State Delivery):**

As the cloud clears at $t = 12\,s$, both the head and flow rate smoothly and rapidly recover to their nominal values, demonstrating excellent hydraulic transient response. During the final partial shading step at $t = 16\,s$, the head and flow rate proportionally adjust to match the new available solar power without any instability. Overall, these hydraulic results conclusively prove that the entire systemfrom the MPPT-controlled PV array down to the physical water pumpoperates with high efficiency and continuous delivery despite severe environmental disturbances.

## 3.5. Conclusion :

In conclusion, Chapter 3 validates the standalone solar water pumping system's performance under changing weather conditions. Combining an advanced FCS-MPC with MTPA optimization for the motor drive ensures highly efficient energy conversion and a stable 400V DC link voltage. Crucially, the direct P&O MPPT algorithm proves superior for this application because it dynamically locks onto the true maximum power point to extract the absolute highest energy possible. Unlike FOCV—which relies on rough mathematical guesses and periodically cuts off power for measurements—P&O delivers continuous, uninterrupted power while adapting to real-time atmospheric shifts. Ultimately, simulation results demonstrate excellent dynamic resilience, showing that the Synchronous Reluctance Motor adjusts smoothly to maintain a continuous water flow even during sudden drops in solar irradiance.

# General Conclusion

This thesis presented a comprehensive study on the modeling, simulation, and advanced control of a standalone Photovoltaic Water Pumping System (PVWPS). To address the critical challenges associated with solar energy intermittency and the need to eliminate expensive, high-maintenance battery storage, a direct-coupling architecture was proposed and rigorously evaluated. The proposed system successfully integrated a photovoltaic array, a DC-DC boost converter, a voltage source inverter, a Synchronous Reluctance Motor (SynRM), and a centrifugal water pump into a cohesive and highly efficient configuration.

The success of the proposed architecture primarily relied on the implemented control strategies. The Perturb and Observe (P&O) MPPT algorithm demonstrated robust capability in extracting the maximum available power under varying atmospheric conditions. More importantly, the application of Finite Control Set Model Predictive Control (FCS-MPC) to the SynRM drive proved highly effective. The simulation results obtained using MATLAB/Simulink conclusively validated that the FCS-MPC algorithm ensured excellent dynamic tracking of stator currents, minimized electromagnetic torque ripple, and maintained system stability even during rapid and severe variations in solar irradiance.

Furthermore, the translation of this electromechanical stability into hydraulic performance provided strong validation of the proposed configuration. Simulations demonstrated that under nominal clear-sky conditions (1000 $W/m^2$), the PVWPS developed a Total Dynamic Head of approximately 30 meters while maintaining a continuous water flow rate of 13.2 $L\cdot min^{-1}$. During simulated heavy cloud cover, the predictive controller effectively managed the energy deficit by allowing the motor to decelerate smoothly without stalling, thereby ensuring uninterrupted water delivery despite significant environmental disturbances.

Although the obtained simulation results firmly establish the viability, efficiency, and high performance of the proposed SynRM-based pumping system, several promising directions remain open for future research and development:

1. **Experimental Validation:** The practical implementation of the proposed FCS-MPC strategy on a real hardware prototype using a physical SynRM and a DSP/dSPACE controller is highly recommended to evaluate real-time computational requirements and practical robustness.

2. **Hybrid Energy Integration:** The integration of an additional renewable energy source, such as a small-scale wind turbine, may be investigated to develop a hybrid energy system capable of extending pumping operation during nighttime or prolonged periods of low solar irradiance.

3. **AI-Based Optimization:** Replacing the conventional P&O MPPT technique with Artificial Intelligence-based approaches, such as Fuzzy Logic or Artificial Neural Networks, could further enhance power extraction performance, particularly under complex partial-shading conditions.

In conclusion, the proposed FCS-MPC-driven SynRM pumping system represents a robust, cost-effective, and environmentally sustainable solution for agricultural water supply applications in remote and off-grid regions.

# References


[1] I. A. Zino, “Renewable Energies in Algeria”, Arab Climate Resilience initiative: Climate Change Impacts in the Arab Region “Towards Sustainable Energy: Resources, Challenges and Opportunities”, Manama, Bahrain, 06-07 October, 2010.

[2] Chandel SS, Naik MN, Chandel R (2015) Review of solar photovoltaic water pumping system technology for irrigation and community drinking water supplies. Renew Sustain Energy Rev J 49:1084–1099.

[3] Chandrasekaran N, Ganeshprabu G, Thyagarajah K (2012) Comparative study of photovoltaic pumping system using a DC motor and PMDC motor. In: International conference on advances in engineering, science and management (ICAESM), Nagapattinam, India, pp 192–132, March 2012.

[4] Betka A (2005) Perspectives for the sake of photovoltaic pumping development in the south. Doctoral Thesis, University of Banta, Algeria.

[5] Sontake VC, Kalamkar VR (2016) Solar photovoltaic water pumping system – a comprehensive review. Renew Sustain Energy Rev.

[6] R. Rajabi Moghaddam "Synchronous Reluctance Motor (SynRM) Design’’ Master thesis of KTH Electrical engineering, 2017.

[7] Ki-ChanKim , Joon Seon Ahn , and Ju Lee, Sung Hong Won, Jung-Pyo Hong ‘’A Study on the Optimal Design of SynRM for the High Torque and Power Factor’’ IEEE transactions on magnetics, vol.43, no.6, june 2007.

[8] Jisha. L.K, P.Thomas, A Comparative Study on Scalar and Vector Control of Induction Motors, IEEE 2013.

[9] C. N. Bhende, S. K. Hota, K. R. Nayak and S. B. Karanki, "Cooperative control of photovoltaic based water pumping system," IET Renewable Power Generation, vol. 14, no.12, pp. 2278-2286, 2020.

[10] T. Lubin "Modélisation et commande de la machine synchrone à réluctance variable, Prise en compte de la saturation magnétique" Thèse de Doctorat de Nancy, avril 2003.

[11] Thierry Lubin, Tahar Hamiti, Hubert Razik, and AbderrezakRezzoug’’Comparison between Finite-Element Analysis and Winding Function Theory for Inductances and Torque Calculation of a Synchronous Reluctance Machine’’IEEE transactions on magnetic, vol.43, no.8, august2007.

[12] S. Mohammad Reza Sadri " variable reluctance motor and drive systems" doctor of philosophy, University of Western Sydney Nepean, October 1995.

[13] Abdallah Bezzini.’’ Commande Prédictive Non Linéaire en Utilisant Les Systèmes Neuro-Flous et les Algorithmes Génétiques’’,Département Génie Electrique, Faculté des Sciences et de la technologie, Université Mohamed Khider – Biskra,2013

[14] L. S. Maraaba, Z. M. Al-Hamouz, and M. A. Abido, “Mathematical modeling, simulation and experimental testing of interior-mount LSPMSM under stator inter-turn fault,” IEEE Trans. Energy Convers., vol. 34, no. 3, pp. 1213–1222, 2018.

[15] M. F. Rahman and S. K. Dwivedi, Modeling, Simulation and Control of Electrical Drives. Institution of Engineering and Technology, 2019.

[16] MODELING AND SIMULATION OF A PHOTOVOLTAIC CELL CONSIDERING SINGLE-DIODE MODELM. AZZOUZI. Faculty of Science and Technology, Ziane Achour University of Djelfa, BP 3117 Djelfa, Algeria.

[17] K. Benlarbi, L. Mokrani, M. S. Nait-Said, “A fuzzy global efficiency optimization of a photovoltaic water pumping system ”, a LSPIE Laboratory.

[18] H. Ali, U. Subramaniam, R. M. Elavarasan, K. Raju, M. Diaz and N. Das and O. Boubaker, "Design of efficient off-grid solar photovoltaic water pumping system based on improved fractional open circuit voltage MPPT technique," International Journal of Photoenergy, vol. 2021, pp. 1-18, 2021.

[19] R.Wills, J. A. Milke, S. Royle, and K. Steranka, Best Practices for Commercial Roof Mounted Photovoltaic System Installation. New York, NY: Springer New York, 2015.

[20] O.Seddik "study and optimization of the operation of a photovoltaic system" Master thesis, University of Ouargla, 2012.

[21] M. LOPEZ, "Contribution to the optimization of a wind energy conversion system for an isolated production unit", Doctoral Thesis of the Doctoral School, Sciences and Technologies of Telecommunications and Systems Information, 2009, France.

[22] A. Darwekar, U. Bhukte, N. Manmode, P. Khawashi, A. Khade and M. Ahmed, "Solar pv based Dc to Dc boost converter for water pumping system," International Researche Journal of Modernization in Engineering Technology and Science, vol. 4, no. 5, pp. 1615-1620, 2022.

[23] M.-Y. Wei and T.-H. Liu, “A high-performance sensorless position control system of a synchronous reluctance motor using dual current-slope estimating technique,” *IEEE Trans. Ind. Electron.*, vol. 59, no. 9, pp. 3411–3426, 2011.